

Magnús T. Gudmundsson · Freysteinn Sigmundsson ·  
Helgi Björnsson · Thórdís Högnadóttir

## The 1996 eruption at Gjalp, Vatnajökull ice cap, Iceland: efficiency of heat transfer, ice deformation and subglacial water pressure

Received: 12 July 2002 / Accepted: 22 April 2003 / Published online: 12 July 2003  
© Springer-Verlag 2003

**Abstract** The 13-day-long Gjalp eruption within the Vatnajökull ice cap in October 1996 provided important data on ice–volcano interaction in a thick temperate glacier. The eruption produced 0.8 km<sup>3</sup> of mainly volcanic glass with a basaltic icelandite composition (equivalent to 0.45 km<sup>3</sup> of magma). Ice thickness above the 6-km-long volcanic fissure was initially 550–750 m. The eruption was mainly subglacial forming a 150–500 m high ridge; only 2–4% of the volcanic material was erupted subaerially. Monitoring of the formation of ice cauldrons above the vents provided data on ice melting, heat flux and indirectly on eruption rate. The heat flux was 5–6×10<sup>5</sup> W m<sup>-2</sup> in the first 4 days. This high heat flux can only be explained by fragmentation of magma into volcanic glass. The pattern of ice melting during and after the eruption indicates that the efficiency of instantaneous heat exchange between magma and ice at the eruption site was 50–60%. If this is characteristic for magma fragmentation in subglacial eruptions, volcanic material and meltwater will in most cases take up more space than the ice melted in the eruption. Water accumulation would therefore cause buildup of basal water pressure and lead to rapid release of the meltwater. Continuous drainage of meltwater is therefore the most likely scenario in subglacial eruptions under temperate glaciers. Deformation and fracturing of ice played a significant role in the eruption and modified the subglacial water pressure. It is found that water pressure at a vent under a subsiding cauldron is substantially less than it would be during static loading by the overlying ice, since the load is partly

compensated for by shear forces in the rapidly deforming ice. In addition to intensive crevassing due to subsidence at Gjalp, a long and straight crevasse formed over the southernmost part of the volcanic fissure on the first day of the eruption. It is suggested that the feeder dyke may have overshot the bedrock–ice interface, caused high deformation rates and fractured the ice up to the surface. The crevasse later modified the flow of meltwater, explaining surface flow of water past the highest part of the edifice. The dominance of magma fragmentation in the Gjalp eruption suggests that initial ice thickness greater than 600–700 m is required if effusive eruption of pillow lava is to be the main style of activity, at least in similar eruptions of high initial magma discharge.

**Keywords** Subglacial eruptions · Ice cauldrons · Heat flux · Magma fragmentation · Efficiency of heat exchange · Ice deformation · Water pressure

### Introduction

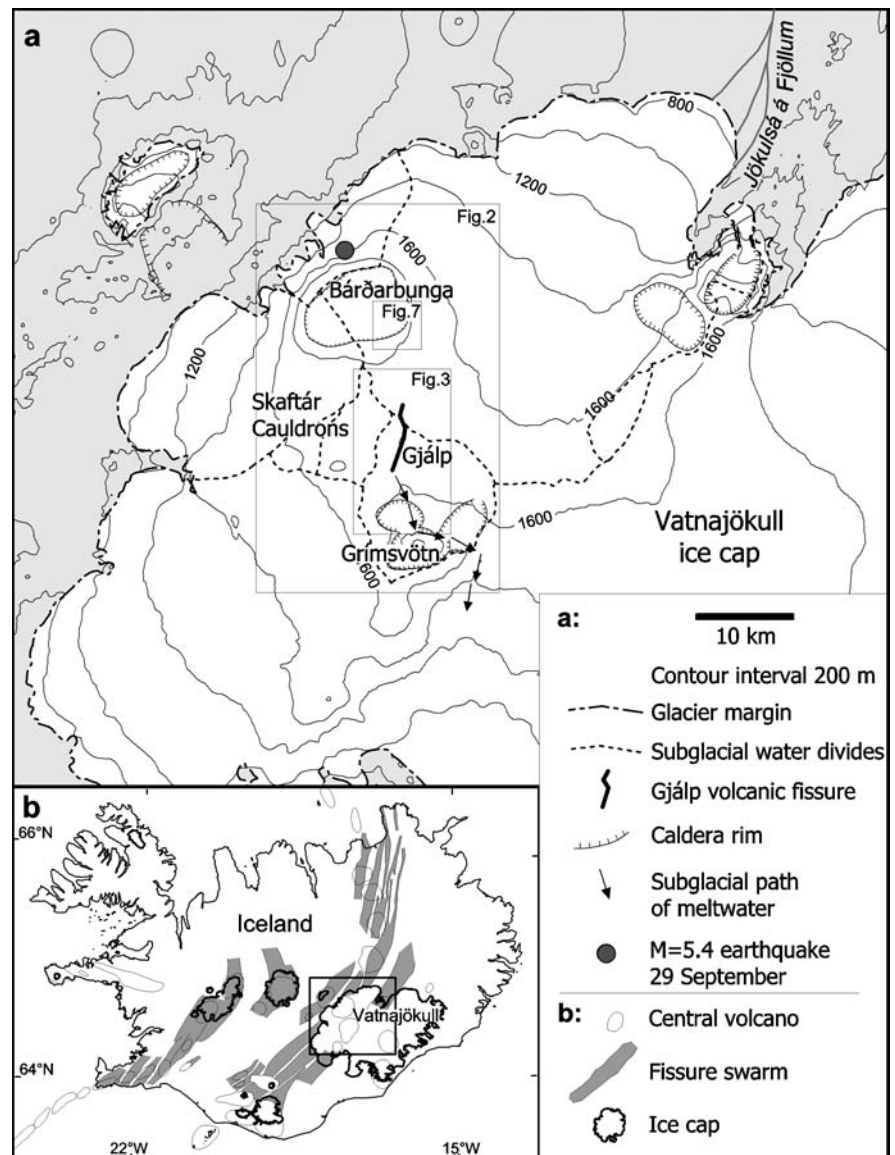
Eruptions within glaciers are characterized by rapid cooling of the volcanic products. Under thick ice covers high confining pressures may lead to effusive eruption and pillow lava formation while quenching and magma fragmentation may be dominant under lower pressures. Due to the rapid cooling, subglacial eruptions tend to create steep-sided mountains made of pillow lava and hyaloclastite (Kjartansson 1943; Mathews 1947; Bemmenlen and Rutten 1955; Jones 1969). The high rates of heat transfer from magma to ice leads to melting of large volumes of ice and large jökulhlaups (outburst floods; Björnsson 1988; Major and Newhall 1989). In Iceland, subglacial volcanic activity played a major role in shaping the landscape during the Pleistocene, creating large fields dominated by tuyas (table mountains) and hyaloclastite ridges. At the present time, parts of the volcanic zones in Iceland are covered by ice caps, and subglacial volcanic activity is frequent (Thorarinsson 1967; Larsen et al. 1998). Subglacial volcanism has shaped the environment

Editorial responsibility: J. Donnelly-Nolan

M. T. Gudmundsson (✉) · H. Björnsson · T. Högnadóttir  
Science Institute, University of Iceland, Hofsvallagata 53,  
107 Reykjavík, Iceland  
e-mail: mtg@raunvis.hi.is  
Tel.: 354-525-5867  
Fax: 354-552-1347

F. Sigmundsson  
Nordic Volcanological Institute, University of Iceland,  
Grensásvegur 50, 108 Reykjavík, Iceland

**Fig. 1. a** Location map of the western part of Vatnajökull (ice cap shown in *white*). **b** A map of Iceland showing fissure swarms and central volcanoes of the volcanic zones (after Einarsson and Saemundsson, 1987). The Gjalp eruption took place midway between the large central volcanoes of Bárðarbunga and Grímsvötn. Ice thickness in the Gjalp area is 500–750 m (see also map of pre-eruption subglacial bedrock topography in Fig. 2). The subglacial water divides prior to the eruption (Björnsson et al. 1992) are shown. The Gjalp fissure crosses the pre-eruption north–south water divide of Vatnajökull but since the southern part of the fissure opened up first (Table 2), meltwater from the eruption drained southwards into the Grímsvötn subglacial lake



in other parts of the world as well, e.g., in western Canada during the last glaciation (Mathews 1947, Hickson 2000). Active volcanoes may also be currently located underneath the West Antarctic Ice Sheet (Blankenship et al. 1993) and large hyaloclastite regions exist on the Antarctic Peninsula (Smellie 1999).

The Gjalp eruption within the Vatnajökull ice cap, Iceland, in October 1996 terminated an almost 50-year-long period of low volcanic activity at Iceland's ice caps. This period was interrupted by only one confirmed short-lived eruption in 1983 within the Grímsvötn caldera in Vatnajökull (Grönvold and Jóhannesson 1984). The 1996 eruption occurred in a somewhat unusual place, subsequently named Gjalp, midway between the two volcanic centers of Grímsvötn and Bárðarbunga (Fig. 1). The eruption lasted from September 30 to October 13 1996 and took place on a 6-km-long fissure under initially 550–750 m of ice. A brief description of the eruption, pointing

out implications for subglacial volcanism, was given by M.T. Gudmundsson et al. (1997) and general description of the activity is provided by Einarsson et al. (1997). The subglacial volcanic ridge formed in the eruption is described on the basis of radio-echo soundings and gravity surveying in M.T. Gudmundsson et al. (2002). Alsdorf and Smith (1999), Björnsson et al. (2001a) and S. Gudmundsson et al. (2002) have used InSAR data to derive post-eruption ice-flow fields within the depressions formed by the eruptions, while Steinthorsson et al. (2000) and Sigmarsson et al. (2000) carried out petrologic and isotopic studies of the erupted tephra. Bödvarsson et al. (1999) compiled a continuous seismic tremor diagram of the eruption.

The Gjalp eruption was the first substantial eruption within a large ice cap to be monitored in any detail. It provided considerable new information on processes occurring in subglacial eruptions under temperate gla-

ciers. In the present paper we give a description of the eruption based on a day-to-day monitoring from an aircraft as well as post-eruption observations and surveying. Magma discharges are estimated from ice melting rates. The efficiency of heat exchange between magma and ice is estimated. The implications of the heat exchange values obtained for possible water ponding in subglacial eruptions are explored. The roles of ice rupture, deformation and subsidence in the course of events are explored, especially the effects of deformation on the subglacial water pressure regime during the eruption.

## Geological background

Vatnajökull has an area of 8,100 km<sup>2</sup> and is 400–700 m thick in most parts (Björnsson 1988). Its western part covers the eastern volcanic zone in Iceland, including parts of several volcanic systems (Fig. 1), each typically consisting of a central volcano and a fissure swarm several tens of kilometers in length (Björnsson and Einarsson 1990). Most of the large central volcanoes have developed calderas and their edifices are major structures with diameters of 15–20 km and relief of about 1,000 m. The most active of these has been Grímsvötn, which holds one of the most powerful geothermal areas in Iceland (Björnsson 1988; Björnsson and Gudmundsson 1993). Geothermal activity in Grímsvötn has created a large depression in the center of the ice cap with ice draining into the depression from an area of 160 km<sup>2</sup>. In the center of the depression is the Grímsvötn caldera with its subglacial lake which drained in jökulhlaups every 4–6 years prior to the Gjalp eruption (Thorarinsson 1974; Björnsson 1988; M.T. Gudmundsson et al. 1995).

Historical records and ice tephrochronology have revealed that the western part of Vatnajökull has the highest eruption frequency of any region in Iceland (Larsen et al. 1998). The high level of activity in the region may be attributed to its location over the center of the Iceland mantle plume (Wolfe et al. 1997). During historical times (since about 900 A.D.) the Grímsvötn volcanic system has been by far the most active. The Bárðarbunga-Veiðivötn system has also shown considerable activity with at least 17 eruptions in the last 800 years (Larsen et al. 1998).

The bedrock under the western part of Vatnajökull is characterized by numerous ridges and mountains considered formed in subglacial volcanic activity, both within the boundaries of the central volcanoes and on their associated fissure swarms (Björnsson 1988; Björnsson and Einarsson 1990; Björnsson et al. 1992, Langley 2000). Although the dates of a large number of historical eruptions within Vatnajökull are known (Thorarinsson 1974), the exact locations of the eruption sites are generally unknown. A noteworthy exception is the subglacial fissure eruption which occurred to the north of Grímsvötn in 1938, when a short ridge with a volume of 0.3–0.5 km<sup>3</sup> was formed under 500–600 m of ice (Gudmundsson and Björnsson 1991, Björnsson 1988).

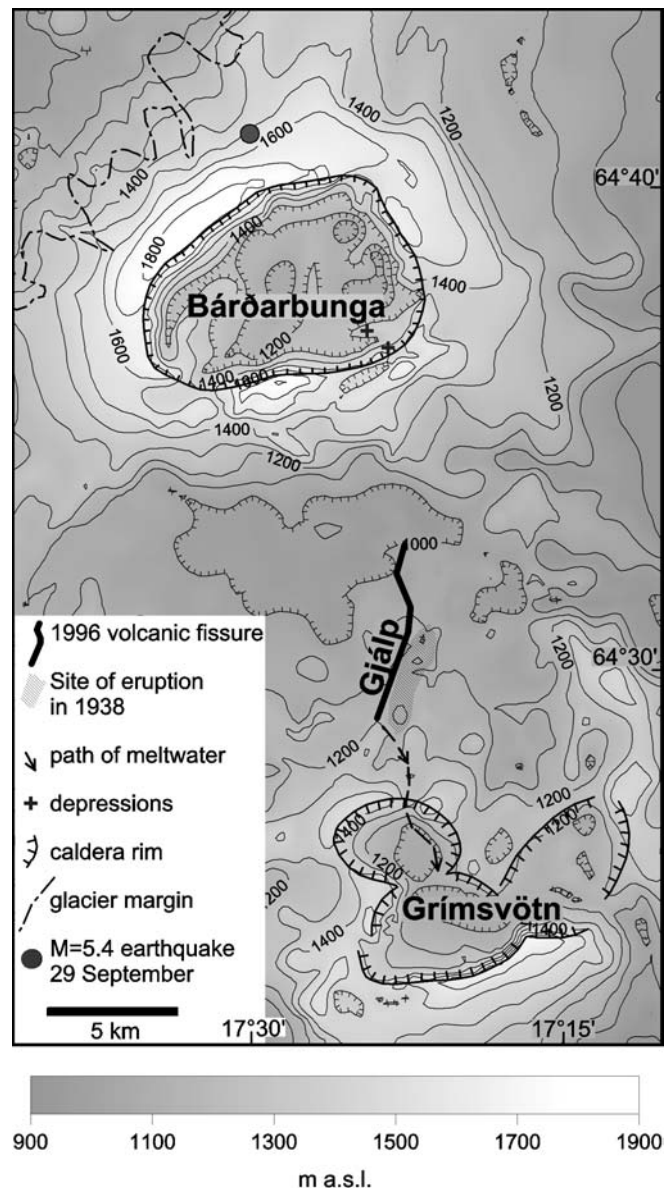


**Fig. 2** Map (contours in m a.s.l.) of the Bárðarbunga–Grímsvötn area showing the pre-1996 bedrock topography as mapped with radio-echo soundings in 1980–1991 (Björnsson 1988; Björnsson et al. 1992) and 1993 (M.T. Gudmundsson et al. 2002). The calderas of Bárðarbunga and Grímsvötn are indicated as well as the inferred subglacial path of meltwater from Gjalp to Grímsvötn. The points in the bedrock directly beneath the two shallow depressions that formed in the SE corner of the Bárðarbunga caldera are marked with crosses. The eruption created a subglacial hyaloclastite ridge (M.T. Gudmundsson et al. 2002) immediately to the west of the 1938 eruption site (see Fig. 12a)

The exact timing of that eruption is not known but large depressions in the ice surface were observed from the air at the end of May 1938. The meltwater drained into the Grímsvötn caldera lake. It caused a jökulhlaup releasing an estimated volume of 4.7 km<sup>3</sup>, out of which 2.7 km<sup>3</sup> are considered to have been meltwater from the eruption site (M.T. Gudmundsson et al. 1995). The 1996 eruption occurred at a similar place as the eruption in 1938 (Fig. 2).

## Glacier hydrology

Melting of ice during eruptions and the drainage of meltwater affects eruption behavior and controls jökulhlaups that may occur. At the base of temperate glaciers, water flow is controlled by the gradient of the static fluid pressure potential, where the most influential factor is the ice overburden pressure. The static potential  $\Phi$  is given by

$$\Phi = \rho_i g \left[ z_s + \frac{\rho_w - \rho_i}{\rho_w} z_b \right] \quad (1)$$

where  $\rho_i$  and  $\rho_w$  are respectively ice and water densities,  $g$  is acceleration due to gravity,  $z_s$  is the ice surface elevation and  $z_b$  is bedrock elevation (Shreve 1972). Water flow is down the gradient of the potential; it follows from Eq. (1) that the ice surface slope is 11 times more influential in determining the gradient than is the bedrock slope. Prior to the 1996 eruption, water divides for western Vatnajökull had been defined on the basis of Eq. (1) (see Fig. 1) and it has been demonstrated that it describes the flow paths of jökulhlaups at Vatnajökull (Björnsson 1986, 1988). This is of considerable importance since it implies that the flow path of jökulhlaups from eruption sites may be predicted.

## Calorimetry

In subglacial eruptions the volcanic fissure and the material erupted cannot be observed directly. Inferences have to be made from trend, length, width and depth of depressions that may form in the ice surface above the eruption site and from what information is available on volume of meltwater draining from the site. In favorable cases, the volume of ice melted by eruptions can be measured and calorimetry used to calculate magma volume. The latent heat of ice melted ( $L_i$ ) is related to the heat content of erupted magma. If the magma solidifies as crystalline rock, the relationship between the total volume of ice melted ( $V_i$ ) and the volume of magma erupted and cooled down to ambient temperature is given by:

$$V_m = \frac{\rho_i L_i V_i}{\rho_m (L_m + C_p \Delta T)} \quad (2)$$

where  $\rho_i$  and  $\rho_m$  are the densities of ice and magma respectively, and  $L_i$  and  $L_m$  are their latent heat of solidification (Table 1). Here,  $C_p$  is the heat capacity of the solidified lava, and  $\Delta T = T_i - T_f$ , where  $T_i$  is the initial magma temperature and  $T_f$  is the ambient temperature. If the magma is fragmented and quenched to glass, crystallization does not happen, and the latent heat is not released. However, the heat capacity of the glass is somewhat higher than that of crystalline lava (Bacon 1977). Using the appropriate heat capacity, the minimum volume of magma may be estimated from

$$V_m = \frac{\rho_i L_i V_i}{\rho_m C_m \Delta T} \quad (3)$$

**Table 1** List of symbols and numerical values of parameters

$\Phi$	Static fluid potential (kPa)
$z_b$	Bedrock surface elevation (m a.s.l.)
$z_s$	Ice surface elevation (m a.s.l.)
$L_i$	Latent heat of solidification of ice, $L_i = 3.35 \times 10^5 \text{ J kg}^{-1}$ (Paterson 1994)
$L_m$	Latent heat of solidification of magma, $L_m = 4.0 \times 10^5 \text{ J kg}^{-1}$ (Spera 2000)
$C_m$	Specific heat capacity of volcanic glass $C_m = 1,100 \text{ J kg}^{-1} \text{ K}^{-1}$ (Bacon 1977)
$C_w$	Specific heat capacity of water $C_w = 4,200 \text{ J kg}^{-1} \text{ K}^{-1}$
$C_p$	Specific heat capacity of crystalline rock
$H$	Height of eruption plume (m)
$Q$	Magma discharge rate ( $\text{m}^3 \text{ s}^{-1}$ )
$\rho_i$	Density of ice ( $\rho_i = 910 \text{ kg m}^{-3}$ )
$\rho_m$	Density of magma ( $\text{kg m}^{-3}$ )
$T_i$	Initial temperature of magma ( $^{\circ}\text{C}$ )
$T_f$	Final temperature of lava/pyroclasts ( $^{\circ}\text{C}$ )
$T_w$	Temperature of meltwater at eruption site ( $^{\circ}\text{C}$ )
$V$	Volume (various subscripts, see Table 3) ( $\text{km}^3$ )
$\dot{E}_i$	Heat transfer from magma to ice (W)
$\dot{E}_w$	Heat transfer from magma to meltwater (W)
$\dot{E}_m$	Influx of heat with magma to vents (W)
$f_i$	Efficiency of heat transfer of ice melting (dimensionless)
$f_m$	Efficiency of heat transfer from magma (dimensionless)
$A$	Ice flow law parameter, $A = 6.8 \times 10^{-24} \text{ s}^{-1} \text{ Pa}^{-3}$ (Paterson 1994)
$n$	Exponent in ice flow law
$d$	Crevasse depth (m)
$h$	Ice thickness (m)
$k$	Ratio of thickness of ductile layer and total thickness of glacier in a subsiding cauldron
$l$	Width of central block in a subsiding ice cauldron (m)
$P_w$	Water pressure at base of ice (kPa)
$\dot{\epsilon}$	Strain (dimensionless)
$\dot{\epsilon}$	Strain rate ( $\text{s}^{-1}$ ), various subscripts
$\tau_{xz}$	Shear stress along a vertical plane striking parallel to volcanic fissure (kPa)
$U$	Ice flow velocity in the vertical direction ( $\text{m s}^{-1}$ )
$\partial U / \partial x$	Strain rate, $\epsilon'_{xz}$ ( $\text{s}^{-1}$ )

Results obtained by Eq. (2) or Eq. (3) are minimum values of  $V_m$  because (1) a fraction of the eruptive activity may be subaerial, and (2) magmatic heat from eruptive products is released over extended periods of time, leading to underestimates of  $V_m$ . Other methods are therefore important in estimating erupted volume such as geophysical surveying of the subglacial edifice coupled with data on volume of subaerially erupted tephra.

## Monitoring and course of events

### Methods

In addition to continuous recording of earthquakes and seismic tremors (Einarsson et al. 1997; Bödvarsson et al. 1999), monitoring of the Gjalp eruption was carried out from aircraft whenever weather permitted. Visual inspection and oblique aerial photography was used to study development of ice surface depressions, crevassing, activity at the subaerial crater, the eruption plume, and fallout of tephra. An important part of the monitoring was the inferring of the elevation of the ice shelf floating on

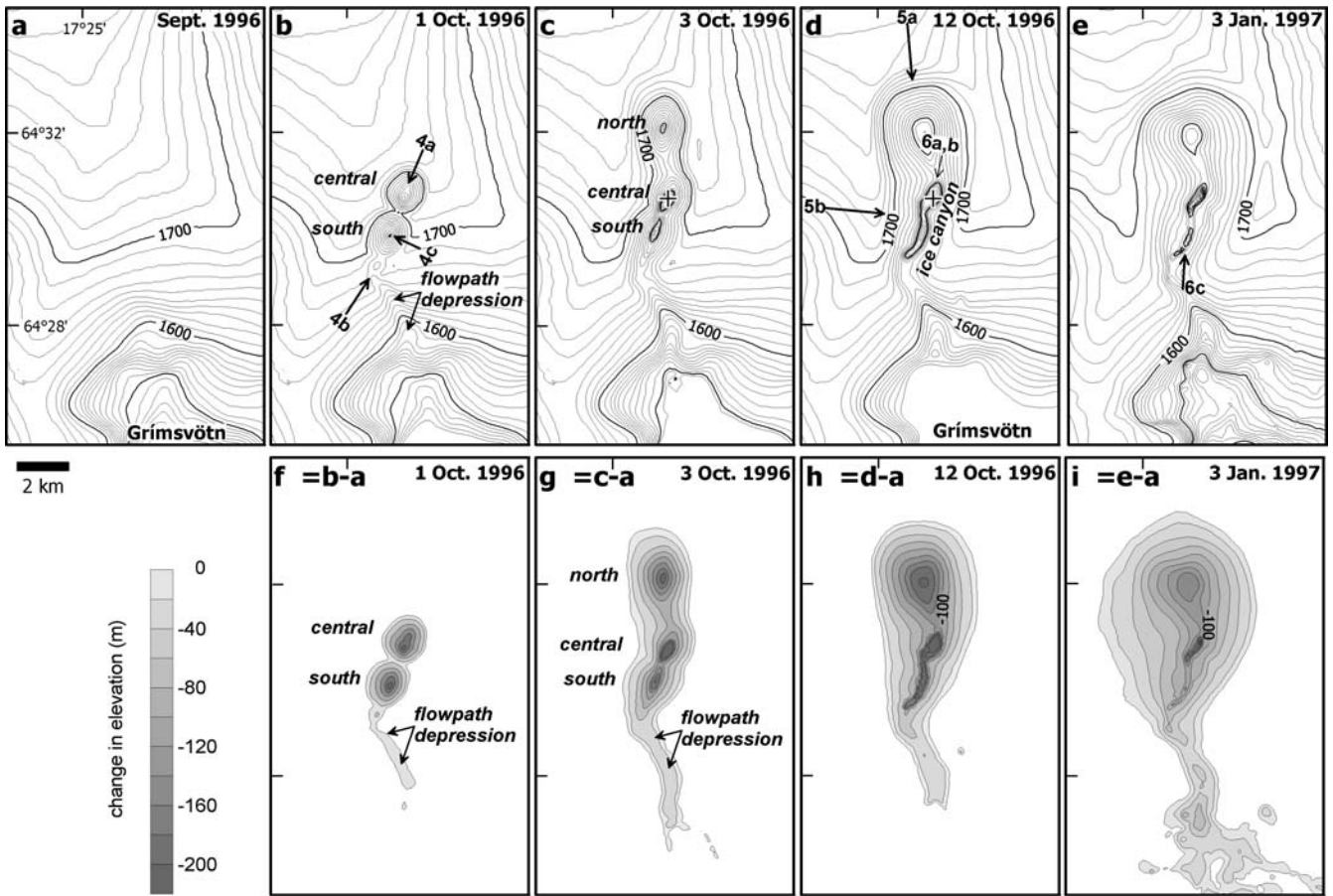


**Fig. 3 a–i** Maps of ice surface in the Gjalp area: **a** before; **b, c, d** during; and **e** after the eruption. The maps in **b–e** are based on airplane radar altimetry and oblique photos. Contour interval 10 m. Parts **f, g, h** and **i** show the differences in elevation between **b** and **a**, **c** and **a**, **d** and **a**, and **e** and **a**, respectively. By 1 October the two cauldrons had reached a depth of about 100 m, the maximum depth on 3 October the maximum depth was over 160 m. The locations of the airplane and the

direction of view in Figs. 4, 5 and 6 are indicated. **i** includes elevation changes due to basal melting in the northern part of Grímsvötn. Before the jökulhlaup on 5–6 November, elevation changes in this area were caused by the rising level of Grímsvötn Lake. The location of the subaerial crater is indicated by a cross in **c** and **d**

the Grímsvötn subglacial caldera lake. The meltwater produced by the 1996 Gjalp eruption flowed into the subglacial Grímsvötn lake as it did in the 1938 eruption. Volume of the lake was calculated from the lake level as the bedrock and ice geometry of the lake are well-known (M.T. Gudmundsson et al. 1995; Björnsson et al. 2001b). This provided a way to estimate volume of meltwater.

An important part of the monitoring was the determination of changes in ice surface elevation, conducted with a Sperry AA220 radar altimeter on board the aircraft. Simultaneous positioning was done with a navigational GPS. Altimeter measurements were done repeatedly along profiles crossing the affected area and changes in the volume of depressions above the subglacial eruptive fissure and the subglacial path of the meltwater could be monitored. The precision of the readings from the altimeter was about 3 m, while the accuracy in elevation determination was about 10 m, about 7–10% of the depth of ice cauldrons. The volume of the ice cauldrons obtained in this way provided a meltwater-volume

estimate independent of the Grímsvötn lake-level measurements.

#### Ice depressions

The eruption caused large changes in ice surface topography through formation of ice cauldrons and other depressions (Fig. 3). Size and form of cauldrons changed quickly with time. The main surface features created in the eruption include:

##### South cauldron:

The southernmost ice cauldron observed on the first day of the eruption (Fig. 3b).

##### Central cauldron:

The cauldron north of the south cauldron, observed on the first day of the eruption (Fig. 3b).

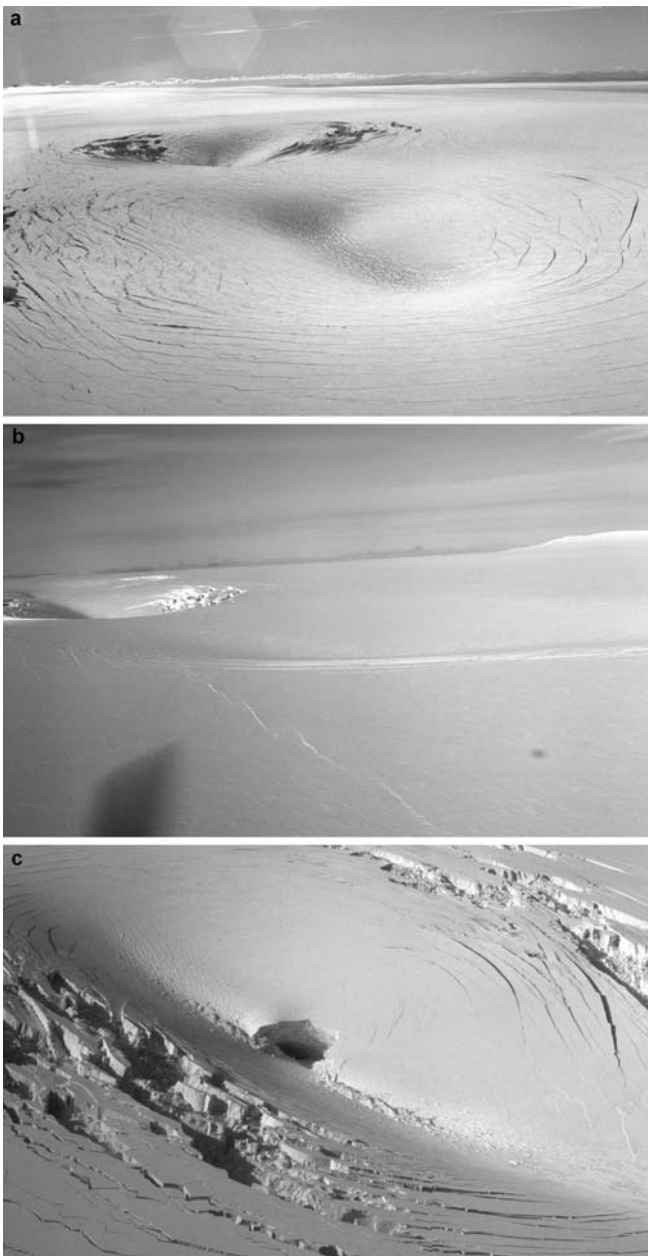


**Fig. 4 a–c** Oblique air photos of the eruption on 1 October. For viewing angles, see Fig. 3b. **a** The ice cauldrons forming at 1200 h on 1 October. View from NNE. The central cauldron where the eruption broke through early the following day is in the *foreground*. The cauldrons were about 2 km wide between the outermost crevasses. **b** View towards NNE from the SSW. The south cauldron is to the left. The en echelon crevasse in the *foreground* is in line with the underlying volcanic fissure and may have formed as a basal crevasse during the opening of the volcanic fissure. **c** Close-up of the south cauldron on 1 October at 1230 h. The collapsed structure in the *center* was 150–200 m wide

#### North cauldron:

The large cauldron that started to form to the north of the central cauldron on 2 October (Fig. 3c).

#### Flow path depression:

A 0.5–0.8 km wide depression between Gjálp and

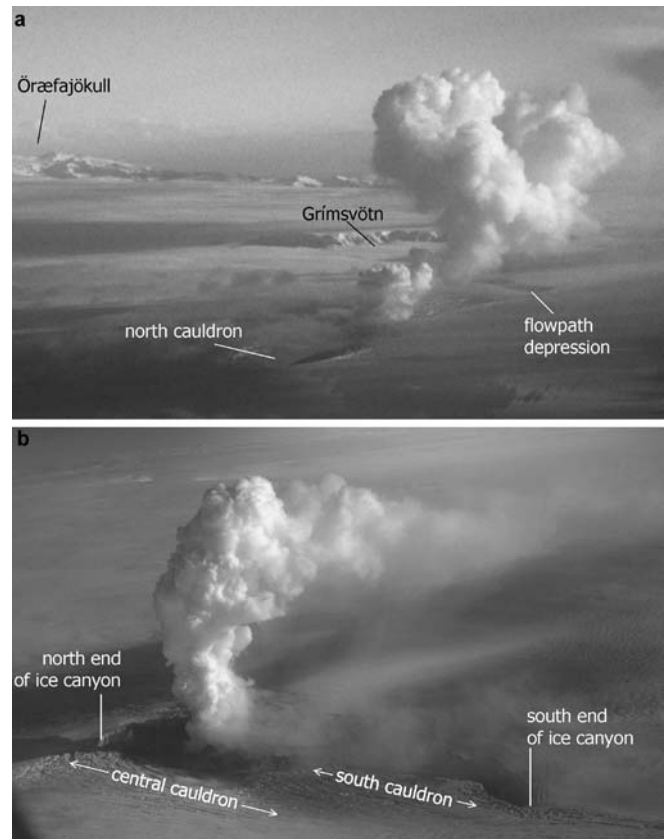


**Fig. 5 a** The eruption site at 1600 h on 3 October. View from the north, elevation of aircraft about 5 km. The north cauldron is about 150 m deep and 3 km wide. Viewing angle is shown in Fig. 3d. **b** The eruption on 12 October. The *dark area* marks the 3.5-km-long ice canyon which is partly obscured by steam. Viewing angle is shown in Fig. 3d

Grímsvötn that had formed on the first day but gradually deepened during the eruption (Fig. 3b).

#### Ice canyon:

The 3.5-km-long canyon with vertical walls that had formed in the ice surface by October 9th, extending through the central and south cauldrons (Fig. 3d).

#### The eruption

The course of events is summarized in Table 2, with references to Figs. 3, 4, 5, 6. Unless otherwise stated, depths of depressions in ice were obtained by radar altimetry, lengths and widths were obtained from GPS aboard the aircraft and the height of the eruption plume was estimated from photos or from airplane barometric altimetry.

As Table 2 shows, the first aerial observations took place in the morning of 1 October, revealing the formation of two cauldrons—south and central—lying on a line trending N20°E. In line with the two cauldrons, a third, very shallow depression was located to the south of the south cauldron. A shallow linear depression—the flow

**Table 2** Course of events at Gjalp, autumn 1996

Date (day/ month)	Description	Fig. No.	Column height (km)
29/9	M=5.4 earthquake in Bárðarbunga at 1048 h. Earthquake swarm starts, later migrating southwards <sup>a</sup>	1	
30/9	Earthquakes. Onset of continuous tremor at about 2200 h— <b>start of eruption</b> <sup>a</sup>		
1/10	Two large depressions/cauldrons forming in ice surface at 1000 h. South cauldron 100 m deep at 1200 hours, central cauldron deepening from 30–50 m at 1200 h to 100 m at 1600 h. Crevasse extending SSW from ice cauldrons with same trend as cauldrons. Ca. 200-m-wide central block in south cauldron collapsing. Meltwater draining subglacially into Grímsvötn. Rise in level of Grímsvötn about 20 m <sup>b</sup>	3b, 4a, b, c	
2/10	Steam observed rising from north cauldron at 0447 h. Explosive issuing of tephra starts at 0518 h. Continuous phreatomagmatic eruption observed at 0800. A new cauldron forming at north end of fissure in afternoon, 3 km long, 2.5 km wide, 20–40 m deep (north cauldron)		3
3/10	Eruption plume at maximum in the morning, 50-km-wide umbrella region. Water observed at site of subaerial crater under 50–80 m high ice cliffs. North cauldron 150 m deep. Rise in level of Grímsvötn, 75 m. Water in Jökulsá á Fjöllum River enriched with chemicals suggesting magmatic influence <sup>c</sup>	3c, 5a, 1	7.5
4/10	Poor visibility. Eruption column pulsating, explosions at about 30-s interval		2
5/10	Poor visibility. Eruption column rising above clouds		3
6/10–7/10	Poor visibility. Eruption column rising above clouds		4.5
8/10	Poor visibility. Eruption column rising above clouds, no height measurement		
9/10	A 3.5-km-long ice canyon observed in the glacier connecting central and south cauldrons. Bottom of canyon 150–170 m below original surface. Width of canyon 150 m except around crater where it is 500–600 m. Water flowing along canyon towards the south	5b	3.5–4.5
10/10	Visibility poor. No data		
11/10	Visibility poor		2
12/10	Width of crevassed area reached 4 km in northern part. Bottom of north cauldron widened by extension towards west. Crater rim observed within the ice canyon. Activity diminishing—explosions less frequent. Total rise in level of Grímsvötn, 105 m	3d, 6a	
13/10	Discrete explosions. End of volcanic tremor in the evening— <b>end of eruption</b> <sup>a</sup>		1
15/10	First clear view of crater. Crater rims are mainly made of ice with thin coating of tephra. Crater conduit in ice ca. 100 m wide and 200–300 m long. Steam rising from crater and ice canyon at the location of the south cauldron. Water rising from depth at north end and sinking at south end of canyon	6b	
17/10	Crater rims cold, covered with new snow		
28/10	Good visibility after spell of bad weather. Water discharge had dropped and two nested canyons had formed within ice canyon—water flowed along the innermost canyon. Two 20-m-deep depressions detected in SE corner of Bárðarbunga. Were not seen during aerial inspection on 1/10 (no visual inspection of this locality 2–27/10)	6c, 7	
5/11–6/11	Total rise in level of Grímsvötn reached 120 m. Water drained from Grímsvötn in a sudden jökulhlaup. Level dropped 170–180 m, to 50–60 m below pre-eruption level as 3.2 km <sup>3</sup> of water were released <sup>b</sup>		
6/11	Short reactivation of magmatic activity at 1345 h when explosions occurred in the south cauldron for 15–20 min, creating a 4-km-high eruption plume. The vent was a few meters wide and the crevasse was ca. 100 m long		

Eruption column height: add 1.6 km to obtain the elevation above sea level

<sup>a</sup> Einarsson et al. (1997)

<sup>b</sup> Gudmundsson et al. (1997)

<sup>c</sup> Kristmannsdóttir et al. (1999)

path depression—extended from the cauldrons southward to the Grímsvötn caldera (Fig. 3b). On 2 October, 31 h after the start of the subglacial eruption travelers saw steam rising from the central cauldron, marking the onset of a subaerial phase. Later that same day, the third main cauldron (north cauldron) started to form to the north of the central cauldron. In the days that followed the cauldrons deepened and grew wider. A thin layer of

tephra was spread over the ice cap, mainly towards the north and east. The eruption continued until 13 October when the last explosive activity was observed; the last volcanic tremors were observed on seismograms in the evening of 13 October (Einarsson et al. 1997).

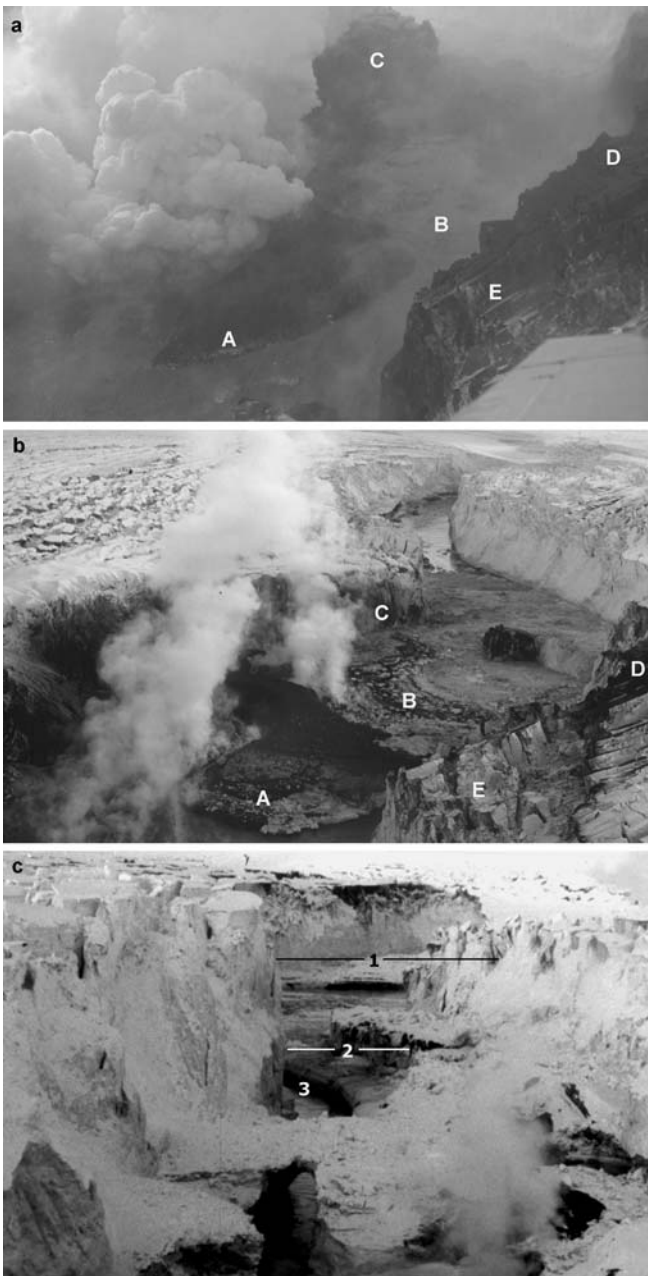


**Fig. 6.** **a** The subaerial crater (marked as *A*) within the ice canyon viewed from the north on 12 October. *B* is water at the bottom the canyon. *C*, *D* and *E* mark spots on the walls and rims of the canyon. The distance between *C* and *D* is 200–250 m. Viewing angle is shown in Fig. 3d. **b** The ice canyon viewed from the north on 15 October, the viewing angle is the same as in **a** but a larger part of the canyon is visible. *A*–*E* are the same locations as in **a**. The photo shows that ice made up the inner walls of the crater. Water flowed southwards along the canyon. Viewing angle is shown in Fig. 3d. **c** The ice canyon on 28 October. Discharge along the canyon *1* had declined and two nested canyons (marked as *2* and *3*) had formed by thermal erosion of the ice. Steam rises from a crevasse located above the southern end of the subglacial edifice. Viewing angle shown on Fig. 3e

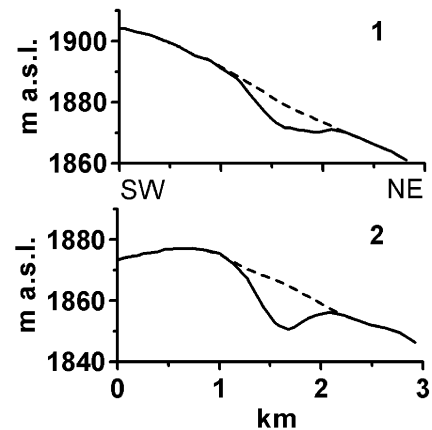
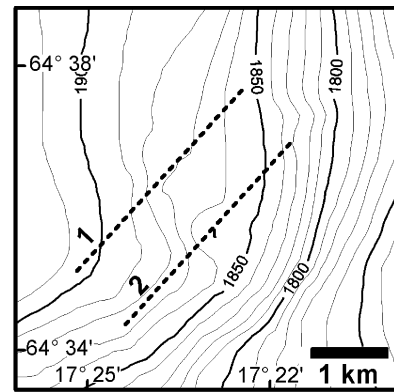


**Fig. 7** Surface contour map of the southeast corner of Bárðarbunga as mapped in over-snow differential GPS traverses in August 1997 and radar altimetry in January 1997. The profiles show the inferred change in ice surface elevation associated with the formation of the cauldrons

### The ice cauldrons in SE corner of Bárðarbunga

Two new ice cauldrons were detected in late October just within the subglacial rim in the SE corner of the Bárðarbunga caldera (Table 2, Fig. 7). They are located 8 km to the north of the northern end of the Gjálp fissure (Fig. 2). It is not clear when these cauldrons formed, perhaps during the Gjálp eruption itself. There is circumstantial evidence that this activity may have happened early in the eruption. Chemical analyses of water in the river Jökulsá á Fjöllum collected on October 3 1996 show that the river was enriched with chemicals suggesting magmatic influence (Kristmannsdóttir et al. 1999); the drainage basin of the river includes the two cauldrons in Bárðarbunga (Figs. 1 and 2). These cauldrons will not be considered further here, but the most likely explanation for their formation is that minor eruptive activity occurred in the SE corner of Bárðarbunga, under 300–500 m of ice (Fig. 2).

## Jökulhlaup, 5–6 November and reactivation of activity

On the evening of 4 November, the ice seal to the east of the Grímsvötn caldera lake broke and the stored meltwater was released in a sudden jökulhlaup. On 6 November the level of Grímsvötn had dropped by 170–180 m as 3.2 km<sup>3</sup> of water had been released from the subglacial lake (M.T. Gudmundsson et al. 1997; Björnsson et al. 2001a). A short reactivation of magmatic activity occurred at the site of the southern cauldron at about 1345 h. Explosions lasted 15–20 min and formed an eruption plume that rose to 4 km in height. This eruptive activity took place through the few meter-wide and about 100-m-long crevasse at the bottom of the ice canyon. There was probably no new magma involved in this activity; it may have been caused by boiling and release of gas as water pressure dropped at the southernmost part of the volcanic fissure when the lake level at Grímsvötn subsided.

### The subglacial hyaloclastite ridge

As residual heat of the volcanic pile under the glacier was gradually released in the months following the eruption, the bottom of the ice canyon at the site of the main crater gradually became lower. By January 1997, the uppermost part of the volcanic pile had become visible. The eastern side was covered by the ice but the uppermost 40 m of the western side were exposed over a 300–400 m long segment of the ridge. Inspection in June 1997 revealed that the exposed part of the ridge was straight and sharp with a slope of 30–35°. It was mainly composed of ash and lapilli-sized glass particles, and less than 1% of the volume was crystalline rock (blocks and bombs). The temperature of the pile was 60–70 °C at 0.5 m depth and slight consolidation was already happening in places (M.T. Gudmundsson et al. 2002). Further inspection of the top of the edifice could not be carried out, since by August 1997 it was submerged in water that had accumulated in the ice canyon (Fig. 3e) over the summer. By the spring of 1998 the edifice had been submerged by ice flow.

Geophysical surveying at Gjalp and Grímsvötn has been used to map the subglacial deposits of the eruption; radio–echo sounding, direct observation in June 1997 and gravity profiling have been reported by M.T. Gudmundsson, et al. (2002). They reveal that the form of the subglacial edifice built up during the eruption is a ridge with a volume of 0.7 km<sup>3</sup> and is highest in the area of the central cauldron where it rises about 500 m over the pre-eruption bedrock. The southern and central parts of the ridge formed in the eruption are steep and narrow while the northern part is wide and of modest relief. Gravity profiling indicates a density of 1,900 kg m<sup>-3</sup> for both north and south parts while a density as low as 1,500–1,600 kg m<sup>-3</sup> is suggested for the central part where the subaerial crater was located. The higher values are consistent with water-saturated uncompacted hyaloclastite, while the density of the central part call for dry

or steam-saturated hyaloclastite, suggesting that considerable residual heat was left in that part of the ridge at the time of the gravity survey in 2000. At Grímsvötn the surveys show that a further 0.07 km<sup>3</sup> of tephra was carried by meltwater into Grímsvötn. The total volume of erupted material is 0.8 km<sup>3</sup>, equivalent to 0.45 km<sup>3</sup> of basalt–icelandite magma of a density of 2,600 kg m<sup>-3</sup>.

### Eruption plume

The use of calorimetry to estimate heat fluxes during the eruption does not take into account the heat lost to the atmosphere through the eruption plume. This effect has to be evaluated. Data on plume height and behavior is given in Table 2. On the basis of these data the plume may be divided into five characteristic stages: initial build-up stage on October 2nd, maximum stage early on 3 October, stable stage 3–10 October, declining stage of intermittent explosions on 11–12 October, and a final steam-plume stage with isolated explosions on the last day of the eruption on 13 October.

During its initial stage on 2 October, intermittent explosions, occurring at intervals of a few minutes, interrupted a continuously fed plume (Table 2). In the strong southerly wind on 2 October, the plume was dark in color and carried a heavy tephra load. It did not form an upwind umbrella region, it was either straight or bent over. The thickest part of the tephra layer formed during the eruption corresponds to the fallout from this initial plume (G. Larsen, personal communication 1997).

During the maximum stage of the plume in the morning of 3 October, it was fed by continuous uprush from an ash-laden jet emanating from the crater. Calm and clear weather facilitated the plume to rise to higher levels (7.5 km height; Table 2). It terminated in a complete umbrella region, the only time it did so during the eruption. The maximum stage of the plume was over in the afternoon of 3 October. The eruption plume was then quasi-steady until 10 October (3–4.5 km height; Table 2). The declining stage of the eruption was characterized by intermittent explosions, each of which generated a discrete plume front. Only isolated explosions occurred during the final stage on 13 October, however, an approximately 1-km-high continuous steam plume was observed throughout this last day of the eruption.

The empirical relationship  $H=1.67Q^{0.259}$ , where  $H$  is the column height in kilometers and  $Q$  the dense rock equivalent discharge rate in m<sup>3</sup> s<sup>-1</sup> (Eq. 5.1 of Sparks et al. 1997), may be used to estimate the magma discharge rate out of the subaerial crater. For the highest plume of 3 October the relation suggests a discharge rate of 300 m<sup>3</sup> s<sup>-1</sup>. A crude estimate of the total volume of subaerially erupted magma is obtained by integrating the discharge rate over time. Although the result should only be regarded as an order-of-magnitude estimate, the obtained value of 0.01–0.02 km<sup>3</sup> was in agreement with volume assessments based on observations of tephra thickness on Vatnajökull (G. Larsen, personal communi-

**Table 3** Volumes of ice melted and volume of volcanic material

Date	$V_d$ (km <sup>3</sup> )	$V_{cr}$ (km <sup>3</sup> )	$V_{p1}$ (km <sup>3</sup> )	$V_{p2}$ (km <sup>3</sup> )	$V_{er}$ (km <sup>3</sup> )	$V_s$ (km <sup>3</sup> )	$V_t$ (km <sup>3</sup> )
1 Oct. 1996	0.22	0.01	0.06	0	(0.11)	0.34	0.39
3 Oct. 1996	0.82	0.06	0.21	0	(0.41)	1.29	1.5
12 Oct. 1996	1.58	0.13	0.40	0	0.80	2.51	2.91
11 Nov. 1996	2.00	0.18	0.47	0.30	0.80	2.98	3.75
3 Jan. 1997	2.20	0.20	0.47	0.30	0.80	3.20	3.97
June 1997	2.30+0.10 <sup>a</sup>	0.15	0.47	0.30	0.80	3.35	4.12
June 1998	2.24+0.25 <sup>a</sup>	0.10	0.47	0.30	0.80	3.39	4.16

<sup>a</sup> The volume added is the estimated net snow accumulation at the surface since the eruption

$V_d$ : Volume of depressions in glacier surface at eruption site

$V_{cr}$ : Volume taken up by crevasses not accounted for in  $V_d$

$V_{p1}$ : Volume of ice melted along the path of meltwater into Grímsvötn

$V_{p2}$ : Volume of ice melted along the path of meltwater out of Grímsvötn on 5–6 November

$V_{er}$ : Volume of erupted material. During the eruption it was assumed that it is in proportion to the sum of the volume of depressions, crevasses and ice melting along the meltwater path. The volume of 0.8 km<sup>3</sup> after the eruption is based on geophysical surveys (M.T. Gudmundsson et al. 2002)

$V_s$ : Total volume of ice melted at eruption site ( $V_s = V_d + V_{cr} + V_{er}$ )

$V_t$ : Total volume of ice melted ( $V_t = V_d + V_{cr} + V_{p1} + V_{p2} + V_{er}$ )

cation, 1997). The subaerial eruption therefore produced only 2–4% of the total volume of magma erupted.

### Development of the volcanic fissure

The form of the volcanic fissure, deduced from the trend of the ice depression, is somewhat unusual. The trend of the southern part (N20°E) is oblique to the dominant trend of volcanic fissures under the western Vatnajökull (about N40°E; Langley 2000). About 1.5 km north of the site of the subaerial crater, the fissure curves and trends a few degrees west of north. The northernmost part trends N15°E and has an offset of almost 1 km relative to the southern part. Variation in bedrock relief prior to the eruption was modest (Fig. 2), about 100 m or less, suggesting that the irregularity in the fissure trend has a tectonic origin rather than being caused by local topography. The northern end of the fissure is about 3 km from the base of the subglacial volcanic edifice of Bárðarbunga. The local stress field of Bárðarbunga may be the main cause for the shape of the fissure. Either loading from the volcanic edifice or high pressure in a magma chamber at Bárðarbunga at the start of the eruption would favor radial fissures if the least principal stress is horizontal and tangent to concentric circles around the volcano. This local stress field would interfere with the regional field that generally favors dyke formation along the dominant strike of roughly N40°E. The sum of the two stress fields could cause the fissure to curve towards Bárðarbunga, as observed.

### Volume of ice melted

The size and extent of ice cauldrons and depressions that formed over the path of the meltwater changed throughout the duration of the eruption. These changes are the principal source of information about the subglacial part

of the eruption. Table 3 gives total melting at various times during and after the eruption. It is based on the volume of depressions on the maps in Fig. 3, estimates of the volume of the volcanic edifice, and the observed changes in ice volume to the south of the eruption site itself, along the inferred path of the meltwater (Fig. 8). The rate of melting was about 0.5 km<sup>3</sup>/day over the first 3 days but declined after that (Table 3); between June 1997 and 1998 the volume of the depressions increased by only 0.04 km<sup>3</sup>. Thus, within a year of the eruption the rate of heat release had declined by three or four orders of magnitude.

### Temperature of meltwater

The subsidence of the ice surface over the subglacial path of the meltwater to the south of Gjálp (Fig. 8, Table 3) shows that a sizable fraction of the magmatic energy was dissipated downstream of the eruption site. The volume of ice melted south of Gjálp is a measure of the energy released along the subglacial flow path by cooling of the fluid draining from Gjálp. The fluid was a mixture of meltwater and tephra. The volume of tephra leaving Gjálp in this way was about 0.07 km<sup>3</sup> according to sediment accumulation in Grímsvötn (M.T. Gudmundsson et al. 2002) while the volume of meltwater was 2.5–3 km<sup>3</sup> (see entries for  $V_s$  in Table 3 for the 12 October and 11 November). Considering also that the specific heat capacity per unit-mass of water is about four times that of volcanic rock (e.g., Spera 2000), the fraction of the heat carried with the sediments can be ignored in the calorimetric estimates of the temperature of the meltwater.

The meltwater lost some of its energy along the path to Grímsvötn (Fig. 8b, area 1), another fraction was lost at Grímsvötn (Fig. 9b, areas 2 and 3), and what remained was released on the first 6–7 km of the subglacial path out of Grímsvötn during the jökulhlaup on 5–6 November

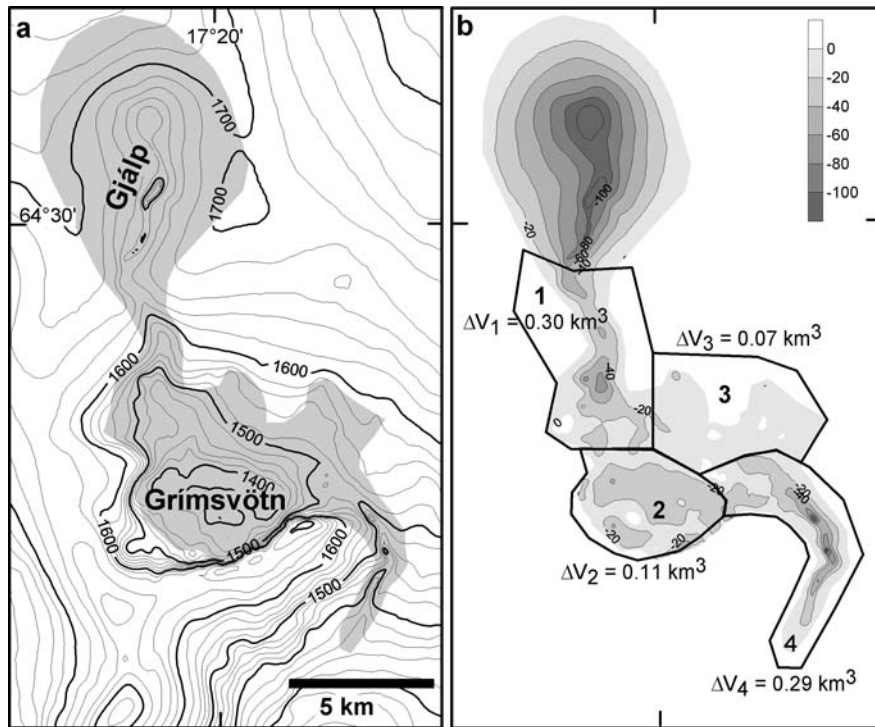


**Fig. 8. a** Map of Grímsvötn and Gjalp in June 1997 based on over-snow differential GPS traverses. The area where the ice surface subsided due to basal melting during the eruption and jökulhlaup in November is shaded. The area can be divided into two regions: (i) the eruption site itself; and (ii) the area to the south of the eruption site, over the inferred path of the meltwater. **b** Map showing changes in elevation between September 1996 and June 1997 due to basal melting caused by the eruption and jökulhlaup. Changes in

the area to the south of Gjalp occurred in October and early November. This area is here divided into four parts: 1 the path from Gjalp into Grímsvötn where  $0.30 \text{ km}^3$  of ice was melted; 2 the ice shelf above Grímsvötn Lake, where melting amounted to  $0.11 \text{ km}^3$ ; 3 the area floated to the north of Grímsvötn where  $0.07 \text{ km}^3$  was melted; and 4 the outlet from Grímsvötn during the jökulhlaup of 5–6 November where the melting amounted to  $0.29 \text{ km}^3$ . The total volume change was  $0.77 \text{ km}^3$  ( $V_{p1}+V_{p2}$ ; Table 3)

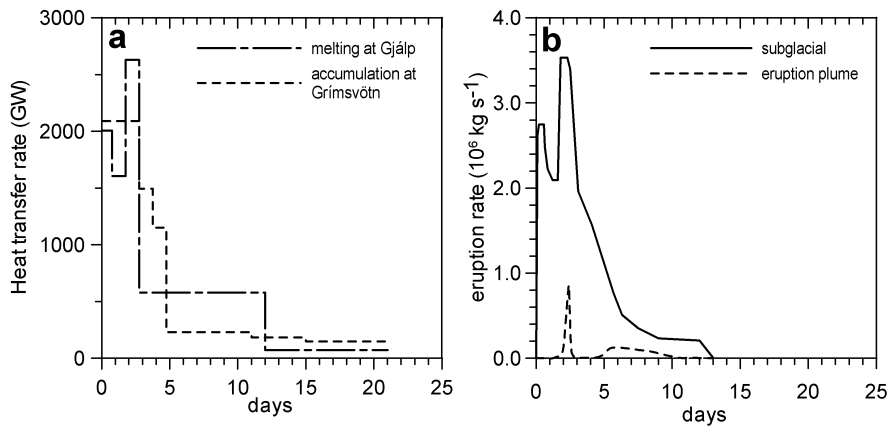


**Fig. 9. a** Heat transfer rate during the Gjalp eruption based on calorimetry using (i) the volume of depressions at Gjalp and (ii) the volume of meltwater accumulated at Grímsvötn. **b** The eruption rate assuming it was proportional to the melting rate. The inferred

total magma volume of  $0.45 \text{ km}^3$  and magma density of  $2,600 \text{ kg m}^{-3}$  is also assumed. The approximate eruption rate of the subaerial eruption is shown for comparison, demonstrating how small a part of the overall activity it was

(Fig. 8b, area 4,  $V_{p2}$  in Table 3). The average temperature of the meltwater at the eruption site ( $T_w$ ) may therefore be estimated from the total volume melted at Gjalp by early November ( $V_S$  for 11 November in Table 3) and the total volume that had been melted along the flow path at the same time ( $V_{p1}+V_{p2}$ ). The initial heat content of the

meltwater was equal to  $\rho_i V_S C_w T_w$ . This heat was available to melt the volume  $V_{p1}+V_{p2}$  of ice ( $\rho_i V_S C_w T_w = \rho_i (V_{p1}+V_{p2}) L_w$ ). The meltwater temperature is then found from  $T_w = (V_{p1}+V_{p2}) L_w / V_S C_w$ . By inserting the appropriate numbers (Tables 1 and 3) the result obtained is  $T_w = 20^\circ \text{C}$ . This is an average value for October 1–5 November. For

the meltwater produced during the eruption itself when convection was most vigorous, this may be an underestimate.

### Heat flow, efficiency of heat exchange and magma discharge

Calorimetry has been used to calculate the heat transfer rate during the Gjálp eruption using the two independent measures of (1) volume of depressions at Gjálp, and (2) meltwater accumulation in the Grímsvötn lake (Fig. 9a). Given the heat transfer rate, the heat flux can be estimated from the size of the area over which the heat exchange occurs. If this is taken as equal to the area of the ridge formed, a minimum estimate of the heat flux in the vent area is obtained. For the first 1.5 days, the heat exchange surface was 3 km<sup>2</sup> but then increased to 5–6 km<sup>2</sup>. This yields a heat flux of 5–6×10<sup>5</sup> W m<sup>-2</sup> for the first 3 days of the eruption, a value too high to be explained by an effusive eruption of pillow lavas.

The rate of heat flux from pillow lavas can be estimated by applying Stefan's problem of solidification and conductive cooling (Höskuldsson and Sparks 1997). In the Gjálp case an initial magma flow rate 2.5–5×10<sup>6</sup> kg s<sup>-1</sup> forming a ridge with a surface area of 3–6 km<sup>2</sup>, would yield a heat flux of 4–8×10<sup>4</sup> W m<sup>-2</sup>. This is an order of magnitude lower than observed. For comparison, fragmentation of the magma into mainly ash-sized glass particles should be capable of causing a much higher heat flux since the thermal diffusion time of particles with diameter ~1 mm is of the order of 1 second (e.g., Wohletz 1983). Thus, if sufficient water is available at the subglacial vent, explosive fragmentation should lead to turbulent mixing of tephra and water and very high heat fluxes (M.T. Gudmundsson et al. 1997). Fragmentation is therefore the most likely eruption mechanism at Gjálp, an inference that is further supported by the gravity modeling results of the edifice being mainly composed of low-density tephra/hyaloclastite, not intermediate-density pillow lava (M.T. Gudmundsson et al. 2002).

#### Magma flow rates

As fragmentation was the dominant eruption mechanism at Gjálp, a strong correlation between magma flow rate and heat transfer rate is likely. A crude estimate of the magma flow rate is shown in Fig. 9b, where it is simply assumed that the eruption rate was at any given time proportional to the melting rate. The total magma volume of 0.45 km<sup>3</sup> is used as a constraint. The two melting estimates in Fig. 9a are merged to yield a higher resolution in Fig. 9b. An estimate of magma discharge ( $Q$ ) through the eruption plume is also provided based on plume height ( $H$ ) and the equation  $H=1.67Q^{0.259}$  (Sparks et al. 1997). The comparison demonstrates the dominant role of subglacial activity in the eruption.

The graph in Fig. 9b undoubtedly gives a skewed image of the actual magma flow since the heat release from previously erupted and partially cooled material is ignored. Thus, a more likely scenario is that magma flow was greater than shown on the graph early in the eruption, but considerably lower at the end when cooling of the previously erupted material probably accounted for a substantial part of the heat transfer rate.

#### Efficiency of heat exchange

The efficiency of the heat exchange can be defined as the ratio of heat released from the magma per unit time and the total heat content of the magma erupted in the same time interval. Since accurate estimates of magma flow rate are not available, neither value can be calculated directly. However, a minimum estimate of the total magmatic heat can be obtained from the total mass of ice melted (Eq. 2 or 3). Maximum and minimum values for the efficiency of heat exchange can be extracted from the ice volumes melted during and by the end of the eruption. A maximum value is obtained by assuming that melting rates during the eruption correspond to magma flow rates as is done in Fig. 9b. An approximate lower bound may be estimated by assuming that virtually all the magma was erupted in the first few days and that melting during the latter part of the eruption was due to cooling of this previously erupted material through conduction and/or convection of water/steam within the volcanic edifice. The true efficiency value should lie between these extremes.

There are two different definitions of efficiency to consider. First, there is the efficiency of heat transfer for ice melting ( $f_i$ ), and secondly, there is the efficiency of heat transfer from magma ( $f_m$ ). In the first case, only energy used to melt ice at the eruption site is considered. For the second case, energy stored in meltwater and released along its path downslope of the eruption site, is also included. Although the efficiency is a measure of how large a fraction of heat carried with the magma is released to the surroundings per unit time, the two efficiency values are here defined as the ratio of ice volumes melted

$$f_m = \frac{\dot{E}_w}{\dot{E}_m} \approx \frac{V_s + V_p}{V_t} \quad (4)$$

$$f_i = \frac{\dot{E}_i}{\dot{E}_m} \approx \frac{V_s}{V_t} \quad (5)$$

Here,  $\dot{E}_w$ ,  $\dot{E}_i$  and  $\dot{E}_m$  are the heat transferred from magma to meltwater, from magma to ice and the influx of heat with magma respectively, while the dots indicate derivatives with respect to time.  $V_s$  is ice melted at the eruption site as before,  $V_p=V_{p1}+V_{p2}$  is the total ice volume melted along the meltwater path, and  $V_t$  is the total volume melted by the eruption (the value used is for June 1997;  $V_t=4.12$  km<sup>3</sup>). Using values for 12 October from

Table 3 for the maximum values and melting as estimated for the first 5 days (Fig. 9a) for the minimum values, the resulting efficiency values are,  $0.50 < f_i < 0.61$  for ice melting and  $0.63 < f_m < 0.77$  for heat release from magma.

### Efficiency and drainage

The efficiency of melting at the eruption site ( $f_i$ ) controls the basal water pressure and the potential for water storage at the eruption site. Theoretical considerations suggest that for a basaltic eruption a heat exchange efficiency ( $f_i$ ) higher than 0.8 is required if the combined volume of meltwater and erupted products is to be less than that of the ice melted (Höskuldsson and Sparks 1997). If efficiency ( $f_i$ ) is less than 0.8, the combined volume of meltwater and volcanics exceeds that of the melted ice, which leads to increasing static fluid potential at the eruption site. Glaciers in general have surface slopes that result in a static fluid potential, which in temperate glaciers drives water towards their margins. The increasing fluid potential should therefore drive meltwater away from the eruption site.

Meltwater that suddenly forms as a result of a subglacial eruption may drain initially as a basal sheet of water. However, such a sheet probably develops into a tunnel (Weertman 1972; Röthlisberger 1972; Nye 1976; Kamb 1987). The well-developed flowpath depression observed at Gjalp by noon on 1 October (Table 2, Figs. 3b and 4b) indicates that a ~0.5-km-wide tunnel had formed within a few hours of the start of the eruption. Experience from jökulhlaups in Iceland and elsewhere suggests that subglacial tunnels do not close again until water pressure has dropped substantially (Björnsson 1988) and that water temperature is a major factor in enlarging tunnels (Nye 1976; Clarke 1982). This indicates that once a pathway has been established away from an eruption site, the path is likely to remain open while being supplied with warm meltwater. Thus for  $f_i < 0.8$  water will have a tendency to drain away more or less continuously, as observed in Gjalp and not accumulate at the eruption site. An exception to this is where conditions for water storage existed before the eruption. This applies to subglacial lakes like Grímsvötn and the Skaftár Cauldrons (Fig. 1) where depressions have formed above subglacial geothermal areas and in some cases where enclosed bedrock depressions exist (Björnsson 1975, 1988).

In a polar ice sheet where the base of the ice is frozen to the bedrock, the situation may be more complicated since brittle fracturing of the ice would probably be required to form subglacial pathways for meltwater. This case is not considered further here.

For Gjalp we have inferred that extensive magma fragmentation did occur. Therefore it is likely that the heat exchange efficiency at Gjalp is at the high end of the range that can be expected in subglacial eruptions. As indicated above, the heat flux in fragmentation is much higher than the flux expected for pillow lava formation given the same magma flow rate. Hence the efficiency of

heat exchange during eruption of pillow lava should be markedly lower than in fragmentation. The increase in water pressure at the eruption site during such an eruption should therefore also favor early or instantaneous drainage of meltwater. The indication is therefore, at least for the early stages of an eruption under temperate glaciers, that the accumulation of the meltwater around the vents is an exception requiring an eruption into a pre-existing subglacial lake.

The expected relatively low efficiency in effusive subglacial eruptions implies that the correlation of ice melting rate and magma flow rate would be still less in an effusive eruption than in an explosive one. Thus, in short-lived effusive eruptions a large part of the thermal energy may be released over a period considerably longer than the duration of an eruption. This would contrast with the behavior of eruptions like that of Gjalp where magma fragmentation is dominant.

---

### Development of ice cauldrons

Although it is the heat from the magma that causes melting and subsidence of the overlying ice, it is important to note that dynamic response of the glacier may have considerable effect on conditions at subglacial volcanic vents. The ice also acts as a constraint on lateral spreading of the volcanic material.

#### Water pressure and cauldron subsidence

The response of the glacier to the melting and drainage caused by the eruption is rapid subsidence (Fig. 3) and inflow of ice towards the vents. The rapid deformation creates large shear stresses in the ice that act to oppose the subsidence. These stresses, together with the water pressure in the meltwater vault that has to overlie the volcanic fissure, balance the downward force of gravity acting on the subsiding ice block. This is important because it implies that water pressure at the vent may be considerably lower than the load of the overlying ice. A highly simplified estimate of the effect of the stress field on water pressure under a collapsing cauldron follows.

Flow of ice by internal deformation is described via Glen's flow law (e.g., Paterson 1994)  $\dot{\epsilon} = A\tau^n$  where  $\dot{\epsilon}$  and  $\tau$  are the effective strain rate and effective shear stress and  $A$  is the flow law parameter (Table 1). It is usually assumed that  $n=3$ . In a subsiding cauldron the surface of the glacier is heavily crevassed which shows that at least the uppermost ice layer is deforming in a brittle manner. If the ice were brittle through most of its thickness, clearly Glen's flow law would not be appropriate for analyzing the mechanics. To estimate the thickness of the brittle layer we use Nye's (1957) equation relating crevasse depth ( $d$ ) to the horizontal strain rate  $\dot{\epsilon}_{xx}$ .

$$d = \frac{1}{\rho_i g} \left( \frac{\dot{\epsilon}_{xx}}{A} \right)^{1/n} \quad (6)$$

where  $\rho_i$  and  $g$  are ice density and acceleration due to gravity, respectively. An approximate estimate of the total stretching of the ice surface can be obtained by measuring widths of crevasses on photos taken at noon on 1 October (Fig. 4a, b). Both the south and central cauldrons had essentially uncrevassed central areas while the flanks were heavily crevassed. The total horizontal strain on the flanks (combined width of crevasses along a profile divided by the length of unstretched profile) was approximately 2–3% for the central cauldron (Fig. 4a) and 7–10% for the south cauldron (Fig. 4c). If this strain accumulated at an even rate since the start of the eruption (14 h) the strain rates were  $5 \times 10^{-7} \text{ s}^{-1}$  and  $1.6 \times 10^{-6} \text{ s}^{-1}$ , yielding crevasse depths of 95–140 m. Although these depths are much greater than the 25–30 m (corresponding to  $\dot{\epsilon}_{xx} \approx 10^{-8} \text{ s}^{-1}$ ) normally observed in glaciers (Paterson 1994), they are minimum values. Slightly greater depths are found if it is assumed that the strain did not accumulate at an even rate, for example if the stretching only occurred during half the period since the start of the eruption. The corresponding doubling of the strain rate results in crevasse depth of 120–170 m. Significantly higher strain rates are unlikely since observations on 1–3 October, when cauldron development was fastest, suggest gradual growth and subsidence of the cauldrons. The calculated crevasse depths suggest that the top 20–25% of the 600-m-thick glacier was brittle while the major part, 75–80% deformed in a ductile manner, indicating that Glen's law is useful in analyzing the mechanics of the cauldron subsidence observed at Gjalp.

Figure 10 shows schematically the forces acting on a subsiding block in the center of a cauldron. We only consider here the case where the ice is subsiding over a volcanic fissure; its length is assumed to be infinite along the  $y$ -axis. The other axes are as shown. Melting occurs mainly under the central block and water is assumed to drain away as it melts. Vertical subsidence increases from zero at the outer edge of the cauldron reaching a maximum at the edge of the central block. Subsidence is taken to be a function of  $x$  only, that is if  $U$  is velocity in the  $z$ -direction  $\partial U / \partial z = \partial U / \partial y = 0$ . This is therefore a case of pure shearing in the vertical direction. By using Glen's flow law and ignoring horizontal stress gradients (which should be permissible for the initial stage of subsidence), it is found that the vertical shear stress  $\tau_{xz}$  is given by:

$$\tau_{xz} = \left( \frac{1}{2A} \frac{\partial U}{\partial x} \right)^{1/n} \quad (7)$$

We want to relate the shear stress with water pressure in the vault. For this we need to consider the force balance in the vertical direction (these are forces per unit length in the  $y$ -direction): (1) the force of gravity acting on the central block  $F_g$ , (2) the upward force opposing gravity caused by the pressure of the underlying water  $F_w$ , and (3)

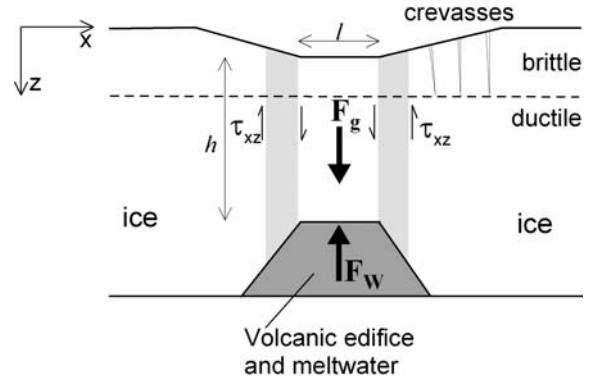


**Fig. 10** Forces acting on a collapsing cauldron. The cauldron is considered to be infinitely long in the  $y$ -direction. The central block is collapsing. An upper ice layer deforms in a brittle way, while a lower ductile layer is assumed to flow according to Glen's law. Crevasses in brittle layer are only shown on one side. The *stippled region* denotes the rather diffuse margin between a subsiding central block and the deforming flanks. See text for discussion

the upwards force caused by shear stress in the ice,  $F\tau = h\tau_{xz}$ . For this simplified case of small vertical subsidence, the force balance equation ( $F_g = F_w + F\tau$ ) can be solved for the water pressure,  $P_w$ :

$$P_w = h \left( \rho_i g - k \frac{2}{l} \left( \frac{1}{2A} \frac{\partial U}{\partial x} \right)^{1/n} \right) \quad (8)$$

Here,  $h$  is the ice thickness in the central block and  $l$  is its width. The first term in Eq. (8) is the lithostatic stress, while the second part is the contribution of the vertical shear stress in the ice. Since the brittle layer is cut by crevasses, it is assumed that it has no shear strength; it only acts as a load on the underlying ductile layer. The term  $k$  accounts for lack of shear stress in the brittle layer, defined as the ratio of the thickness of the ductile layer and the total thickness of the glacier (for Gjalp  $k=0.7-0.8$ ). The derivation of Eq. (8) rests on the assumption that a central block of width  $l$  exists; if  $l \ll h$  the assumption of the force balance is no longer valid. One way of estimating  $l$  is by considering the melting at the base since the central part should suffer much less shearing as melting by the eruption removes ice. Thus, the main movement above this central region should be vertical subsidence. At first this width is similar to that of the subglacial ridge at any given time. Under the southern cauldron where eruptive activity seems to have stopped early in the eruption, the ridge formed is 400–500 m wide (M.T. Gudmundsson et al. 2002). The several hundred meter wide crevasse-free area in the center of the cauldrons (Fig. 4a, c) also supports the existence of a central block; moreover the center of the cauldrons collapsed when subsidence was well advanced (M.T. Gudmundsson et al. 1997). The collapse structure in the center of the southern cauldron (Fig. 4c) had a diameter of about 200 m. We therefore propose that for the Gjalp eruption a width ( $l$ ) in the range of 200 to 500 m is appropriate. During the earliest stage of an eruption the

height of the central block ( $h$ ) should only be slightly smaller than the initial ice thickness.

For Gjalp, the subsidence in the first 16 hours was 50–100 m in the center of the cauldrons directly above the volcanic fissure, but zero at the outer margins 1 km away from the center (Fig. 3b). This gives  $\partial U/\partial x \approx (75 \text{ m}/1,000 \text{ m}/16 \text{ h}) \approx 1.3 \times 10^{-6} \text{ s}^{-1}$  and  $\tau_{xz} \approx 460 \text{ kPa}$ .

If  $h=500 \text{ m}$ ,  $\rho_i=910 \text{ kg m}^{-3}$  and  $k=0.75$ , the resulting water pressure for  $l=200 \text{ m}$  is 2.7 MPa about 1.8 MPa less than the weight of the overlying ice block. For  $l=500 \text{ m}$  the corresponding water pressure is 3.7 MPa, about 0.7 MPa less than the load of the overlying ice.

The above numbers, although somewhat arbitrary, suggest that water pressure in the vault underneath a cauldron during early stages of collapse is of the order of 1 MPa less than the load of the overlying ice. By ignoring horizontal stress gradients we overestimate  $\tau_{xz}$  in Eq. 8 which leads to an underestimation of the absolute water pressure under the cauldron. This effect is small while cauldron depth is an order of magnitude less than the ice thickness.

The result that water pressure in the vault underneath a collapsing cauldron is less than the load of the ice thickness is important for subglacial eruptions since it suggests that fragmentation and explosive activity may start earlier under an ice cap than it would in a lake or ocean with the same initial basal pressure. On a different scale, Tuffen et al. (2002) considered possible implications of small low-pressure cavities at the glacier base for small-volume rhyolitic eruptions and suggested they might influence the trajectory of rising magma.

#### Glacier rupture during volcanic fissure opening

The crevasse extending towards SSW along the trend of the volcanic fissure (Figs. 3b, 4b) was located in a previously uncrevassed area. The crevasse trends obliquely to ice surface contour lines and both pre- and post-eruption ice-flow lines. Thus, it is not related to regional ice flow. Neither can it be explained with subsidence; crevasses caused by subsidence can be seen curving along edges of depressions further away in Fig. 4b. The most plausible explanation for this crevasse seems to be rupture of the glacier from the base to the surface during the opening of the volcanic fissure. We believe this crevasse started as a basal crevasse and cut through 500–600 m of ice. Using Nye's formula (Eq. 6), setting  $d=500 \text{ m}$  and solving for strain rate, the result is  $\dot{\epsilon}_{xx} \approx 10^{-8} \text{ s}^{-1}$ . This must be regarded as the minimum strain rate required to form a 500-m-deep crevasse.

Formation of a tensional basal crevasse in the ice above a subglacial volcanic fissure depends on the coupling of the glacier to the underlying bedrock. If the coupling is sufficiently strong, large tensional stresses will build up in the ice and resulting high strain rates may open a crevasse (Fig. 11a). Furthermore, Wilson and Head (2002) have suggested that dykes may overshoot the

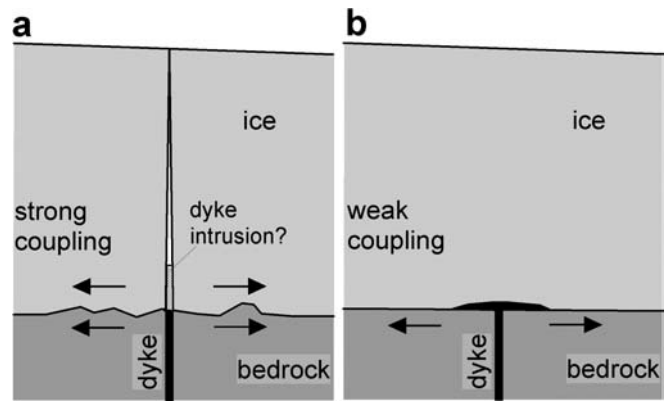


**Fig. 11a, b** Possible formation of a basal crevasse when a dyke reaches the ice–bedrock interface. If coupling between ice and bed is strong the glacier may rupture, possibly up to the surface as in **a**. In **b** coupling at the interface is weak, the ice will not rupture and magma may initially spread some distance along the interface. The arrows indicate the relative movement of the bedrock and ice in the two examples

bedrock–ice interface and intrude some distance into the overlying ice. If the coupling is weak, slip may occur along the ice–bedrock interface without the formation of a basal crevasse (Fig. 11b).

The observation of a glacier rupture related to the opening of the Gjalp eruptive fissure, suggests strong coupling of the glacier to the bedrock at the eruptive site (variable topography on the ice–bedrock interface ensures this), and high strain rates. Magnitude estimates of strain rates show that an extensive basal crevasse is indeed likely to have been formed at Gjalp. A common dyke width is  $\sim 1 \text{ m}$  (Gudmundsson 1983), and eruptive fissures in Iceland have been observed to grow and reach its final length over a period of 1 h, during which the feeder dyke is likely to gradually open up. The strain rate near a dyke tip for these conditions would be  $\sim 1 \text{ h}^{-1}$ , or  $\sim 3 \times 10^{-4} \text{ s}^{-1}$ , which is just about the strain rate required to form a 500-m-high crevasse according to Nye's formula reaching through the ice at the site of the observed glacier rupture. However, the basal crevasse formed above an eruptive fissure is likely to be significantly shorter as the strain rate decays rapidly away from the dyke tip, resulting in reduced height for the fissure. In the Gjalp case, the observation of a glacier rupture at the surface of a 500-m-thick ice may actually suggest that a dyke intruded some distance into the ice, with a crevasse forming only above the dyke tip in the upper part of the glacier.

If a basal crevasse forms at the start of a subglacial eruption it influences the course of events throughout the eruption. The possible effects of such a crevasse, both generally and with special reference to the Gjalp eruption include:

1. If a several hundred-meter-high crevasse of a width of  $\sim 1 \text{ m}$  opens up suddenly in a glacier, the melting rate may not be able to keep up with the increase in void volume. The crevasse may for a short period be largely

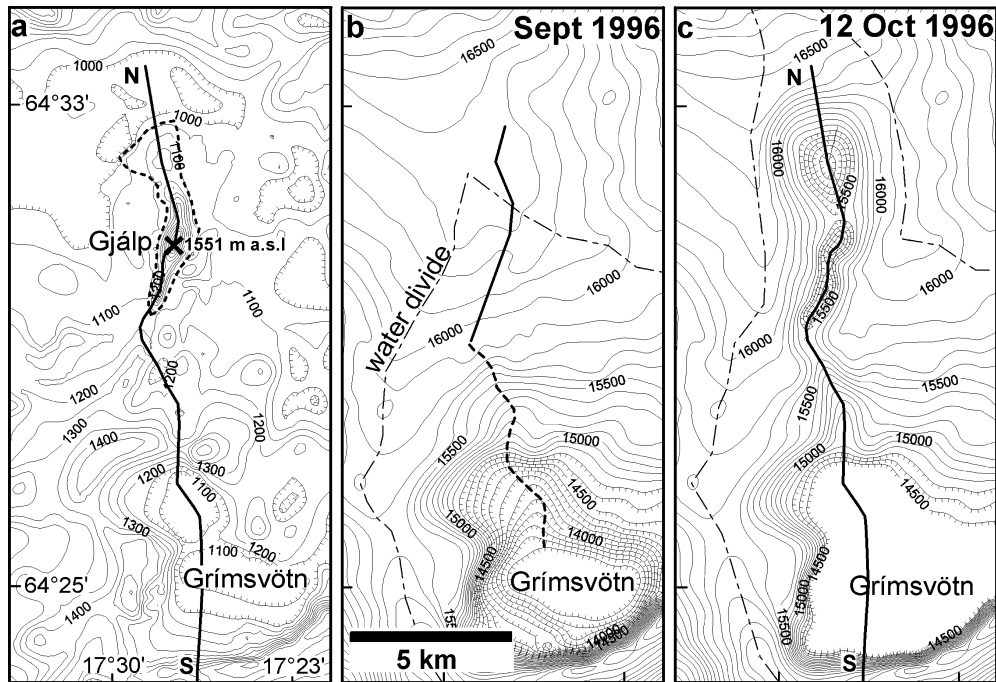


**Fig. 12.** **a** Post-eruption bedrock with the edifice formed in the eruption indicated by the dotted line. The profile shown in Fig. 14 is indicated by the *thick line*. **b** Static fluid potential contours (in kPa) based on pre-eruption ice surface and bedrock contours. The water divide between Grímsvötn and the surrounding areas is shown. The *solid heavy line* is the volcanic fissure. Its northernmost

part was to the north of the pre-eruption water divide. The *dashed line* shows the subglacial flow path of the meltwater as marked by depressions in the ice surface (Figs. 3, 8). **c** Static fluid potential on 12 October. The development of the depressions has extended the water drainage basin of Grímsvötn to the south slopes of Bárðarbunga

air-filled, leading to a short-lived reduction in water pressure at the magma/water interface. Meltwater produced should, however, rise quickly upwards in the crevasse, while the lower part of the crevasse should also close rapidly by ice deformation. The closure time (from horizontal deformation rate) predicted by Glen's flow law is only a few hours for a 1-m-wide air-filled crevasse at a depth of 250 m, but much less at the surface.

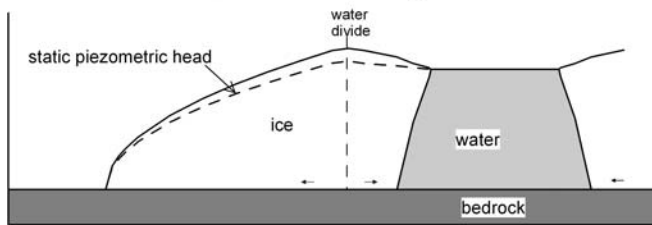
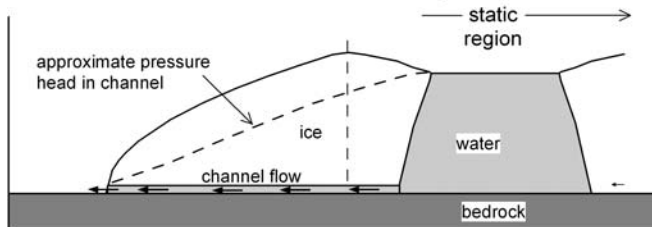
2. Although a crevasse may close rapidly by ice deformation, it will persist for some time as a weakness in the ice. Such a weakness may provide an explanation for opening of a steep or semi-vertical channel for the meltwater from the southern side of the ice canyon to the base in the latter stages of the eruption. Hydrostatic pressure in a water column would be greater than in an equally high ice column due to the higher density of the water. Thus, the water pressure should have been sufficient to open the crevasse again, establishing a drainage channel to the base of the glacier.
3. At the bottom of the southern part of the ice canyon, a line of narrow holes gave off steam during the weeks after the eruption (Fig. 6c). The ice thickness at this site was 150–300 m at the end of the eruption. Here the basal crevasse may have acted as a passage for steam and hot water, with thermal erosion of the crevasse walls keeping pace with closure by ice deformation.
4. The crevasse may also explain why water from the northernmost part of the volcanic fissure rose to the

surface and flowed along the ice canyon in the latter stages of the eruption. Water pressure may have been sufficient to re-open the crevasse, in this case for water to flow upwards to the surface.

### Subglacial water flow and water pressure

As Fig. 12 shows, the meltwater from the eruption site flowed along a path down the gradient of the fluid potential (Eq. 1). The minor role of the bedrock topography is displayed in Fig. 12 where the inferred flow path is shown on the bedrock map. This demonstrates applicability of the static fluid potential to describe the basal hydrology of temperate glaciers. As the eruption progressed, the development of the cauldrons altered the potential (Fig. 12c). Flow of water along the fissure and the initial meltwater path continued but by 12 October a closed dip in the potential had developed over the northern part of the fissure. This suggests that meltwater may have been trapped at that site.

The slope of the fluid potential defines the direction of water flow at the base, but as discussed earlier the large volumes of meltwater that drain away from an eruption site will quickly form a tunnel. Drainage will occur along the tunnel while it remains open but the static fluid potential does not predict the pressure at points within the tunnel. This is demonstrated in Fig. 13 where the static potential describes the seepage of water at the bed. After

**a** Static conditions, before water escapes from the lake**b** Channel flow, after water starts flowing out of the lake

**Fig. 13a, b** Hypothetical cross sections through an ice-dammed lake and its ice dam in a temperate glacier. In **a** static conditions prevail. Before a pathway out of the lake is formed, water seeps along the bed as predicted by the fluid flow potential (e.g., Björnsson 1988). In **b** a pathway for water has been established. The water level of the ice-dammed lake is the same as in **a** but water flows along the bed in a subglacial tunnel through the ice dam. The broken line shows the approximate basal water pressure for the two cases

water starts to drain out of the reservoir through a tunnel, the direction of flow is determined by the pressure difference between the ends of the tunnel. This is important to bear in mind for Gjálp since the water flowed along a tunnel into the Grímsvötn subglacial lake.

### Water pressure at vents

A key question regarding subglacial eruptions is how water pressure at a volcanic vent is related to ice thickness. We try to evaluate this for the Gjálp eruption, even if the uncertainties are large. Above, it has been suggested that both the collapse of ice cauldrons and the possible formation of a basal crevasse act to reduce the water pressure. The level of the Grímsvötn lake is a further constraint. Since water flowed from Gjálp to Grímsvötn throughout the eruption the piezometric head at Gjálp must have been higher than at Grímsvötn. An upper limit for the piezometric head is that which gives a pressure equal to the ice overburden pressure underneath the cauldrons. For October 1st the difference between these limits within the ice cauldrons was about 200 m. The situation for 1 October and 12 October is shown in Fig. 14. In the regions termed as static, flow velocity is assumed to be sufficiently slow for pressure to be determined by Eq. (1) while tunnel flow is assumed between the static regions.

The estimates of water pressure under the cauldrons according to Eq. (8) suggest underpressure of 0.7–

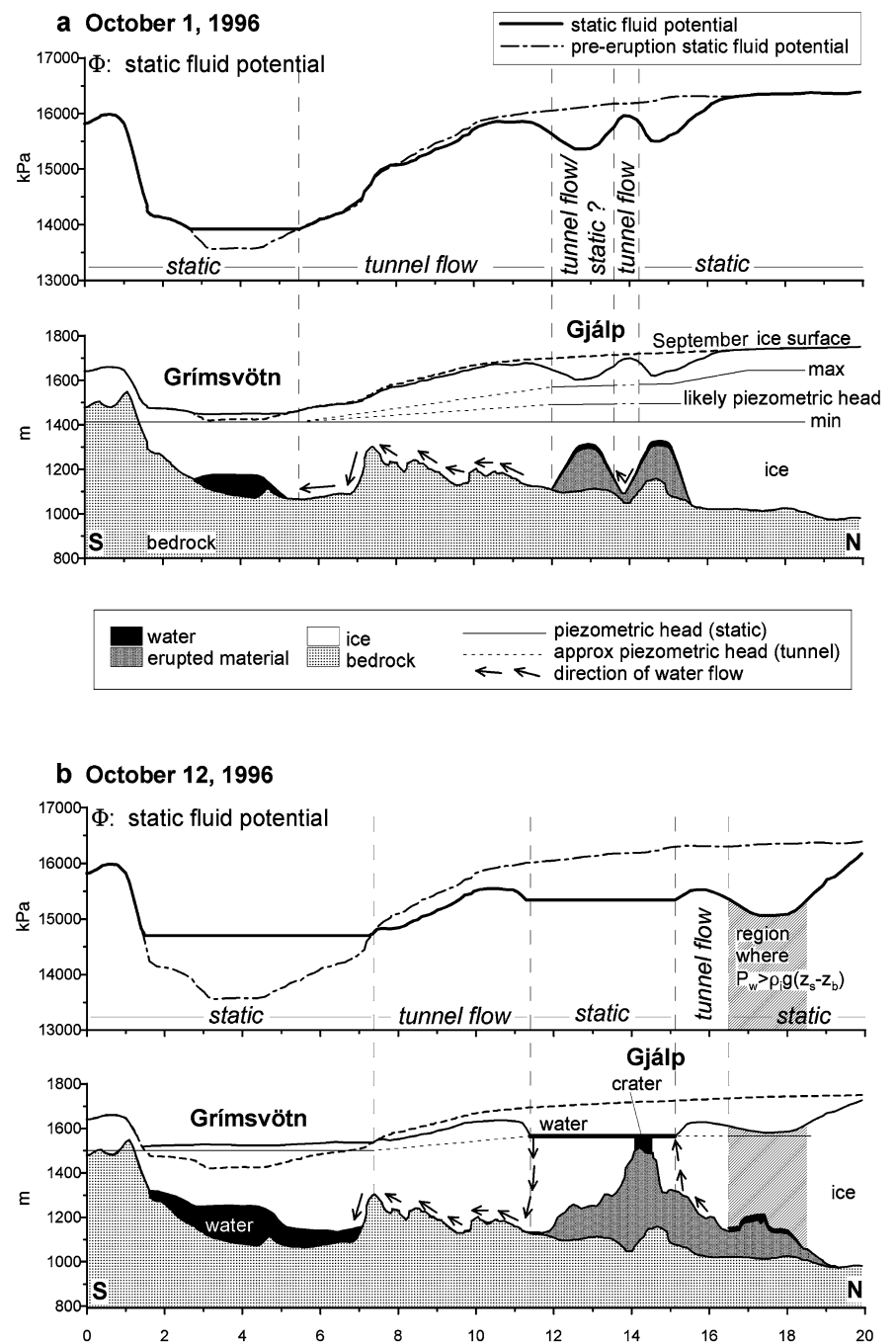
1.8 MPa, equivalent to a piezometric head 70–180 m below the upper limit. Although estimates of water pressure based on Eq. (8) should be regarded as very approximate, they are, however, plausible. In Fig. 14a the pressure reduction due to subsidence for the south and central cauldrons was taken as 1 MPa on 1 October. Our estimate of the height of the volcanic edifice on 1 October is somewhat uncertain. However, since eruption under the southern cauldron seems to have ceased after the first day, the edifice is assumed to have reached its full height at that place on 1 October. Thus, the edifice under the southern and central cauldrons was recorded as 200–250 m high on 1 October. This suggests that the water pressure at the vents at the top of the edifice on that day was 1–3 MPa, with 2 MPa being a plausible value. The thickness of the water layer on top of the edifice is unknown, perhaps a few tens of meters.

By 12 October the level of Grímsvötn had risen to 1,500 m. At the same time the cauldrons had subsided further. Moreover, since water was flowing along the ice canyon at the eruption site, the piezometric head was determined by its level. A somewhat higher water pressure in the northern cauldron was required to sustain the pressure gradient that drove water upwards into the canyon at its northern end. In Fig. 14b a region is indicated in the northern cauldron where the water pressure at the base exceeded the calculated load of the overlying ice. The water pressure at the vent under the northern cauldron was about 4 MPa on 12 October. Accumulation of meltwater at this site was probably minor since no subsidence events can be related to the release of water after the eruption; the depth of the cauldron reached a maximum on 12 October.

The available data do not allow for accurate estimates of the variations of water pressure at the vents throughout the eruption. There are, however, clear indications on variations and these can be summarized as follows:

- South and central cauldrons: When the eruption started, a crevasse opened up, possibly causing a brief initial low-pressure phase. The water pressure rapidly increased to at least 4–4.5 MPa, as required for water to flow along the bed towards Grímsvötn. As the height of the edifice increased the pressure was gradually reduced to 2 MPa after 14–18 hours (Fig. 14a). After 30 h, when the subaerial eruption commenced, water pressure at the vent was probably no more than 0.5–1 MPa while the absolute piezometric head remained similar. After 3 October, the pressure at the subaerial vent decreased with increased elevation of the edifice being close to atmospheric by the end of the eruption.
- North cauldron: The initial basal water pressure on 2 October was 4–6.5 MPa. As subsidence started, this pressure may have stayed at 4 MPa, even being reduced to 3 MPa at the vent on 3 October due to the increased height of the edifice. As the subsidence stabilized and stopped, water pressure may have risen again. On 12 October the pressure at the vent was close

**Fig. 14a, b** Development of volcanic edifice, flow path of meltwater and changes in static fluid potential from 1–12 October. The *narrow lines* mark the piezometric water head at Grímsvötn and Gjálp. **a** 1 October: the *upper panel* shows the static fluid potential as defined from Eq. (1) before the eruption (*broken line*) and on 1 October (*heavy solid line*). In the *lower panel* the minimum piezometric head is set as equal to the level of Grímsvötn; the maximum possible level is the floating level of ice within the cauldrons. The likely level was evaluated as 1 MPa below the maximum. Although the depressions are lows in the potential, the existence of an open subglacial flow path between depressions and to Grímsvötn ensured continuous flow from the cauldrons. **b** 12 October: at this late stage in the eruption the basal water pressure was sufficient to keep the bottom of the northern cauldron floating. Subglacial flow of water from the northern cauldron was probably hampered by the existence of the edifice; it may have acted as a dam, forcing water to flow over it. The piezometric head was observed in open water reservoirs (termed *static* in the figure) but the heads of the closed conduits (termed *tunnel flow*) are stipulated qualitatively



to 4 MPa (Fig. 14b). The region where basal water pressure exceeded ice overburden pressure, indicating floating of the ice by 12 October is shown in Fig. 14. It is in this region that the edifice is 1.5–2 km wide (E–W) and only 150–200 m high (Figs. 12a, 14b), which differs radically from the steep and narrow south and central parts. This difference in shape has been explained by the spreading of the edifice under the north cauldron late in the eruption. Floating of the ice removed the mould confining the edifice and as a result it spread sideways (M.T. Gudmundsson et al. 2002).

The eruption produced mainly fragmented material (M.T. Gudmundsson et al. 1997, 2002, this work). The above constraints on water pressure show that fragmentation of magma of the type erupted at Gjálp occurred at water pressures of 3–4 MPa, equivalent to water depths of 300–400 m. These are considerably higher pressures than for example assumed by Jones (1969, 1970) for subglacial volcanoes in SW Iceland.

## The ice canyon

The flow of water along the ice canyon on the surface over the southern part of the volcanic fissure was a somewhat surprising phenomenon. Clearly, water pressure in the north cauldron was high enough to drive water up to the canyon, and pressure at the central cauldron was sufficiently high to make the canyon a favorable pathway. A possible explanation would be if the edifice in the central cauldron acted as a dam for subglacial water flow from the north. The possible pathways for meltwater from the northern part were along the side of the edifice, seepage through the edifice and flow over its top. Late in the eruption, flow along the side of the edifice may have been blocked by slumping of the loose pyroclasts. Coupled with the decreasing potential gradient between Gjálp and Grímsvötn (Fig. 14) this would have led to increasing basal water pressure upstream of the central part of the edifice, opening up a pathway to the surface and leading to the formation of the ice canyon. Seepage by Darcian flow through the edifice would have been too ineffective to transport the large volumes of meltwater. Melting by the warm water within the canyon would have led to formation of the almost vertical ice walls of the canyon. The nested canyons (Fig. 6c) formed as the discharge fell after the eruption. Photos taken in October of 1996 show that the thermal erosion rate within the canyon in the weeks after the eruption was on the order of 2 m/day.

---

## Summary and conclusions

Analysis of data on the Gjálp eruption has demonstrated that behavior of eruptions within glaciers can be complicated and influenced by many factors. Eruption rate, mode of heat transfer from magma, ice thickness, ice deformation, initial ice rupturing and hydrological constraints all play an important role. The key findings are:

- Heat flux from magma to ice was up to  $5\text{--}6 \cdot 10^5 \text{ W m}^{-2}$ , which is an order of magnitude higher than obtained from cooling models for pillow lavas. The dominant mechanism of heat transfer was therefore fragmentation and quenching of the magma into glass. This is supported by estimates of the density of the edifice (M.T. Gudmundsson et al. 2002).
- The efficiency of heat exchange between magma and ice is found to have been 0.50–0.61. This parameter describes the instantaneous heat transfer from magma to ice at the eruption site. An efficiency of 0.8 or higher is required if conditions for water accumulation at eruption site are to develop (Höskuldsson and Sparks 1997). It is likely that at Gjálp, heat exchange efficiency was near the high end of the spectrum to be expected for subglacial eruptions. This suggests that conditions for water accumulation during subglacial eruptive activity are rarely met except in pre-existing subglacial lakes. A related efficiency parameter, that of heat exchange between magma and meltwater is

found to have been 0.63–0.77. The higher value is because energy used to heat the meltwater to about 20 °C is included here. The thermal energy of the meltwater is dissipated along the path of the meltwater downslope of the eruption site.

- Analysis of forces acting at a subsiding ice cauldron shows that water pressure underneath it is less than the weight of the overlying ice. The difference is taken up by shear forces created as the ice deforms during collapse. This implies that water pressure at subglacial volcanic vents may be considerably less than suggested by ice thickness. For Gjálp the difference between ice load and water pressure may have been 1–2 MPa, implying that water head at the vents was 100–200 m less than would have been the case for static conditions.
- A crevasse ruptured the glacier above the volcanic fissure during its opening. In the southern part this crevasse reached from the base to the surface of the glacier. The eruption feeder dyke may have overshot the bedrock–ice interface and intruded the lower part of the glacier. The associated intense deformation created the crevasse. This crevasse seems to have been a pathway for meltwater during the eruption.
- The water pressure at the vents in Gjálp and dominance of magma fragmentation indicate that confining pressure as high as 3–4 MPa (equivalent to 300–400 m water depth) was not sufficient to suppress fragmentation of the magma. Considering that the initial ice thickness was 550–750 m, this may suggest that a still greater ice thickness is required for pillow lava formation to be dominant in subglacial eruptions, at least for the magma discharge rates of an order of  $10^3 \text{ m}^3 \text{ s}^{-1}$  inferred for the early part of the Gjálp eruption.

**Acknowledgements** We would like to thank Gudrún Larsen, Finnur Pálsson, John Smellie and Tómas Jóhannesson for their useful discussions. Constructive and helpful comments by reviewers Jim Head and Joe Walder improved the quality of this paper. The aerial field observations during and after the eruption were made with the assistance of the Iceland Civil Aviation Authority, especially chief pilot Snaebjörn Guðbjörnsson, and the helicopter service Þyrluþjónustan and pilot Jón K. Björnsson. Fieldwork on the glacier in 1997, 1998 and later was done with the aid of the Iceland Glaciological Society and the National Power Company of Iceland. Financial support for this project was obtained by a special grant from the Icelandic Government and the Icelandic Public Road Administration.

---

## References

- Alsdorf DE, Smith LC (1999) Interferometric SAR observations of ice topography and velocity changes related to the 1996, Gjálp subglacial eruption, Iceland. *Int J Remote Sensing* 20:3031–3050
- Bacon CR (1977) High temperature heat content and heat capacity of silicate glasses: experimental determination and a model for calculation. *Am J Sci* 277:109–135
- Bemmelen RW van, Rutten MG (1955) Table mountains of northern Iceland. *EJ Brill, Leiden*, pp 1–217

- Björnsson H (1975) Subglacial water reservoirs, jökulhlaups and volcanic eruptions. *Jökull* 25:1–11
- Björnsson H (1986) Surface and bedrock topography of ice caps in Iceland mapped by radio-echo soundings. *Ann Glaciol* 8:11–18
- Björnsson H (1988) Hydrology of ice caps in volcanic regions. *Societas Scientiarum Islandica*, 45, Reykjavík, pp 1–139
- Björnsson H, Einarsson P (1990) Volcanoes beneath Vatnajökull, Iceland: evidence from radio-echo sounding, earthquakes and jökulhlaups. *Jökull* 40:147–168
- Björnsson H, Gudmundsson MT (1993) Variations in the thermal output of the subglacial Grímsvötn Caldera, Iceland. *Geophys Res Lett* 20:2127–2130
- Björnsson H, Pálsson F, Gudmundsson MT (1992) Vatnajökull, northwestern part, 1:100,000, subglacial surface map. National Power Company and Science Institute, Reykjavík
- Björnsson H, Rott H, Gudmundsson S, Fischer A, Siegel A, Gudmundsson MT (2001a) Glacier–volcano interactions deduced by SAR interferometry. *J Glaciol* 47:58–70
- Björnsson H, Pálsson F, Flowers GE, Gudmundsson MT (2001b) The extraordinary 1996 jökulhlaup from Grímsvötn, Vatnajökull, Iceland. *American Geophysical Union Fall Meeting. Eos Trans AGU* 82:47
- Blankenship DD, Bell RE, Hodge SM, Brozena JM, Behrendt JC, Finn C (1993) Active volcanism beneath the West Antarctic ice sheet and implications for ice-sheet stability. *Nature* 361:526–529
- Böðvarsson R, Rögnvaldsson ST, Slunga R, Kjartansson E (1999) The SIL acquisition system— at present and beyond year 2000. *Phys Earth Planet Inter* 113:89–101
- Clarke GKC (1982) Glacier outburst flood from “Hazard Lake”, Yukon Territory, and the problem of flood magnitude prediction. *J Glaciol* 28:3–21
- Einarsson P, Saemundsson K (1987) Earthquake epicentres 1982–1985 and volcanic systems in Iceland. Map 1:750,000. Menningarsjóður, Reykjavík
- Einarsson P, Brandsdóttir B, Gudmundsson MT, Björnsson H, Grönvold K, Sigmundsson F (1997) Center of the Icelandic hotspot experiences volcanic unrest. *Eos* 78:369–375
- Grönvold K, Jóhannesson H (1984) Eruption in Grímsvötn: course of events and chemical studies of the tephra. *Jökull* 34:1–11
- Gudmundsson A (1983) Form and dimensions of dykes in eastern Iceland. *Tectonophysics* 95:295–307
- Gudmundsson MT, Björnsson H (1991) Eruptions in Grímsvötn 1934–1991. *Jökull* 41:21–46
- Gudmundsson MT, Björnsson H, Pálsson F (1995) Changes in jökulhlaup sizes in Grímsvötn, Vatnajökull, Iceland, 1934–1991, deduced from in situ measurements of subglacial lake volume. *J Glaciol* 41:263–272
- Gudmundsson MT, Sigmundsson F, Björnsson H (1997) Ice–volcano interaction of the 1996 Gjalp subglacial eruption, Vatnajökull, Iceland. *Nature* 389:954–957
- Gudmundsson MT, Pálsson F, Björnsson H, Högnadóttir T (2002) The hyaloclastite ridge formed in the subglacial 1996 eruption in Gjalp, Vatnajökull, Iceland: present-day shape and future preservation. In: Smellie JL, Chapman M (eds) *Ice–volcano interaction on Earth and Mars*. Geological Society, London Spec Publ. 202, pp 319–335
- Gudmundsson S, Gudmundsson MT, Björnsson H, Sigmundsson F, Rott H, Carstensen JM (2002) Three-dimensional glacier surface motion maps at the Gjalp eruption site, Iceland, inferred from combining InSAR and other ice-displacement data. *Ann Glaciol* 34: 315–322
- Hickson CJ (2000) Physical controls and resulting morphologic forms of Quaternary ice-contact volcanoes in western Canada. *Geomorphology* 32:239–261
- Höskuldsson Á, Sparks RSJ (1997) Thermodynamics and fluid dynamics of effusive subglacial eruptions. *Bull Volcanol* 59:219–230
- Jones JG (1969) Intraglacial volcanoes of the Laugarvatn region, southwest Iceland, I. *Q J Geol Soc Lond* 124:197–211
- Jones JG (1970) Intraglacial volcanoes of the Laugarvatn region, southwest Iceland, II. *J Geol* 78:127–140
- Kamb B (1987) Glacier surge mechanism based on linked cavity configuration of the basal water conduit system. *J Geophys Res* 92:9083–9100
- Kjartansson G (1943) *Árnesingasaga: The geology of Árnessýsla district*. Árnesingafélagid, Reykjavík, pp 1–250
- Kristmannsdóttir H, Björnsson A., Pálsson S, Sveinbjörnsdóttir ÁE (1999) The impact of the 1996 subglacial volcanic eruption in Vatnajökull on the river Jökulsá á Fjöllum, North Iceland. *J Volcanol Geotherm Res* 92:359–372
- Langley K (2000) A morphological investigation of volcanic activity beneath Vatnajökull, Iceland, interpreted from radio-echo sounding data. MS Thesis, University of Iceland, pp 1–129
- Larsen G, Gudmundsson MT, Björnsson, H (1998) Eight centuries of periodic volcanism at the center of the Iceland Hot Spot revealed by glacier tephrostratigraphy. *Geology* 26:943–946
- Major JJ, Newhall CH (1989) Snow and ice perturbation during historical volcanic eruptions and the formation of lahars and floods. *Bull Volcanol* 51:1–27
- Mathews WH (1947) “Tuyas.” Flat topped volcanoes in northern British Columbia. *Am J Sci* 245:560–570
- Nye JF (1957) The distribution of stress and velocity in glaciers and ice sheets. *Proc R Soc Lond Ser A* 239:113–133
- Nye JF (1976) Water flow in glaciers: jökulhlaups, tunnels and veins. *J Glaciol* 76:181–207
- Paterson WSB (1994) *The physics of glaciers*. Pergamon/Elsevier, Kidlington, pp 1–480
- Röthlisberger H (1972) Water pressure in intra- and subglacial channels. *J Glaciol* 62:177–203
- Shreve RL (1972) Movement of water in glaciers. *J Glaciol* 62:205–214
- Sigmarsson O, Karlsson HR, Larsen G (2000) The 1996 and 1998 subglacial eruptions beneath the Vatnajökull ice sheet in Iceland: contrasting geochemical and geophysical inferences on magma migration. *Bull Volcanol* 61:468–476
- Smellie JL (1999) Lithostratigraphy of Miocene–Recent, alkaline volcanic fields in the Antarctic Peninsula and eastern Ellsworth Land. *Antarct Sci* 11:347–363
- Sparks RSJ, Bursik MI, Carey SN, Gilbert JS, Glaze LS, Sigurdsson H, Woods AW (1997) *Volcanic Plumes*. Wiley, London, pp 1–574
- Spera FJ (2000) Physical properties of magma. In: Sigurdsson H (ed) *Encyclopaedia of volcanoes*, Academic Press, New York, pp 171–190
- Steinthorsson S, Hardarson BS, Ellam RM, Larsen G, (2000) Petrochemistry of the Gjalp 1996 subglacial eruption, Vatnajökull, SE Iceland. *J Volcanol Geotherm Res* 98:79–90
- Thorarinsson S (1967) Hekla and Katla. The share of acid and intermediate lava and tephra in the volcanic products through the geological history of Iceland. In: Björnsson S (ed) *Iceland and the Mid-Ocean Ridges*. *Soc Sci Islandica* 38:190–197
- Thorarinsson S (1974) Vötnin Stríð. Saga Skeiðarárhlaupa og Grímsvatnagosa [The swift flowing rivers: the history of Grímsvötn jökulhlaups and eruptions]. Menningarsjóður, Reykjavík, pp 1–254
- Tuffen H, Pinkerton H, McGarvie DW, Gilbert, JS (2002) Melting at the glacier base during a small-volume subglacial rhyolitic eruption: evidence from Bláhnúkur, Iceland. *Sediment Geol* 149:183–198
- Weertman J (1972) General theory of water flow at the base of a glacier or ice sheet. *Rev Geophys Space Phys* 10:287–333
- Wilson L, Head JW (2002) Heat transfer and melting in subglacial basaltic volcanic eruptions: implications for volcanic deposit morphology and meltwater volumes. In: Smellie JL, Chapman M (eds) *Ice–volcano interaction on Earth and Mars*. Geological Society, London Spec Publ. 202, pp 5–26
- Wohletz KH (1983) Mechanisms of hydrovolcanic pyroclast formation: grain-size scanning electron microscopy, and experimental studies. *J Volcanol Geotherm Res* 17:31–64
- Wolfe CJ, Bjarnason ITh, VanDecar JC, Solomon SC (1997) Seismic structure of the Iceland mantle plume. *Nature* 385:245–247